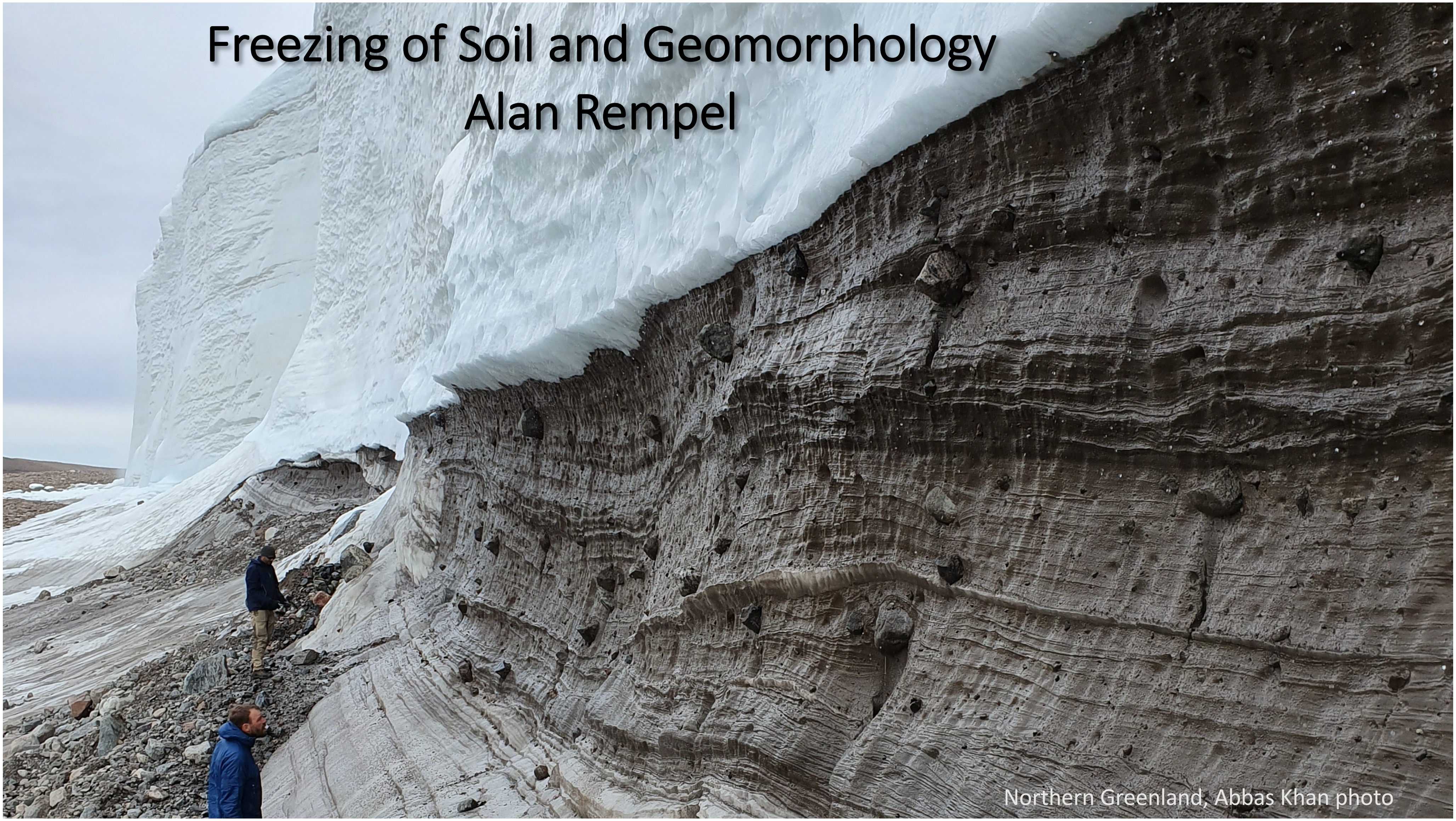
Freezing of Soil and Geomorphology
Alan Rempel
Northern Greenland, Abbas Khan photo

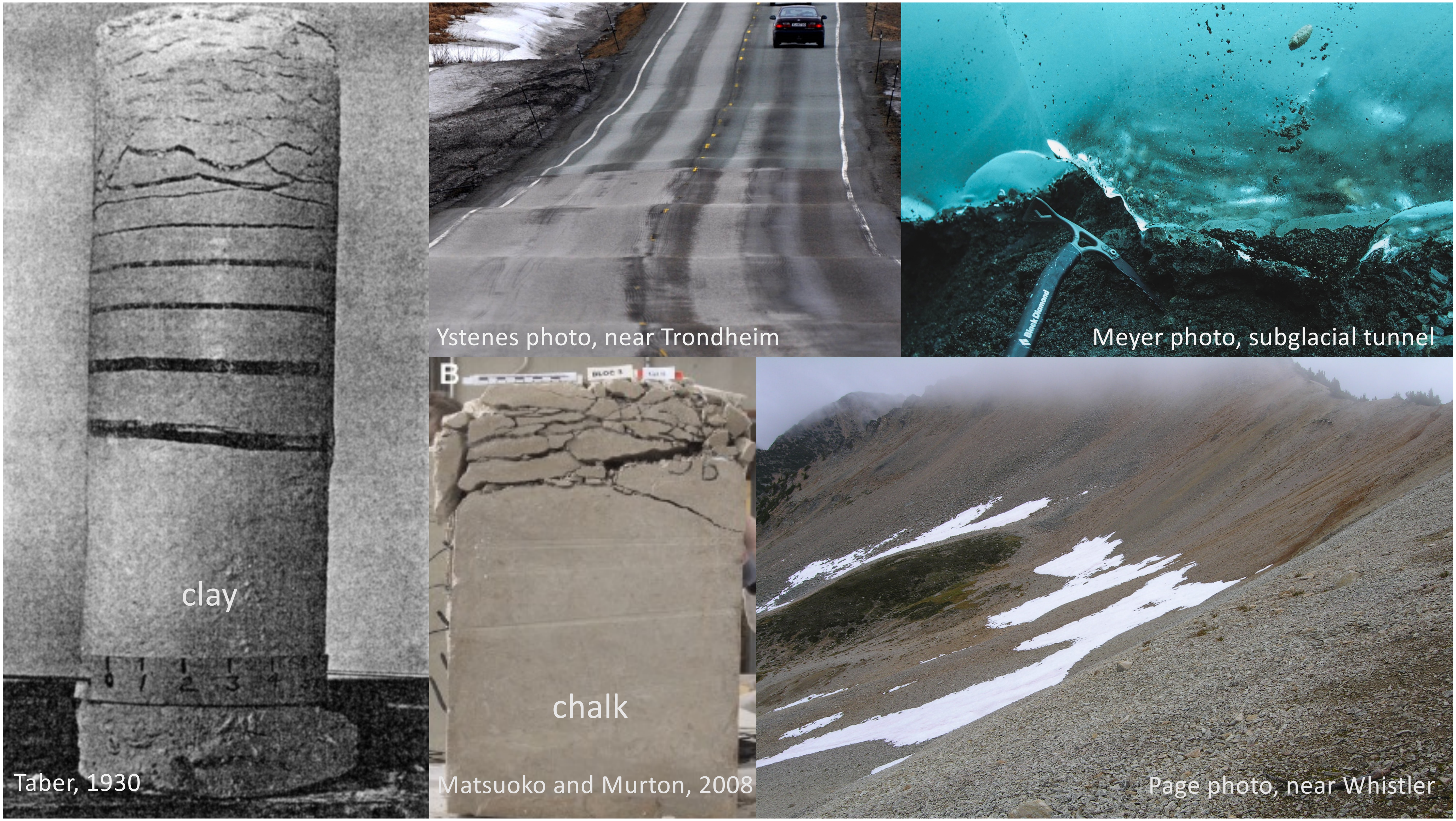
clay
Taber, 1930
Ystenes photo, near Trondheim
Meyer photo, subglacial tunnel
B
chalk
Matsuoko and Murton, 2008
Page photo, near Whistler

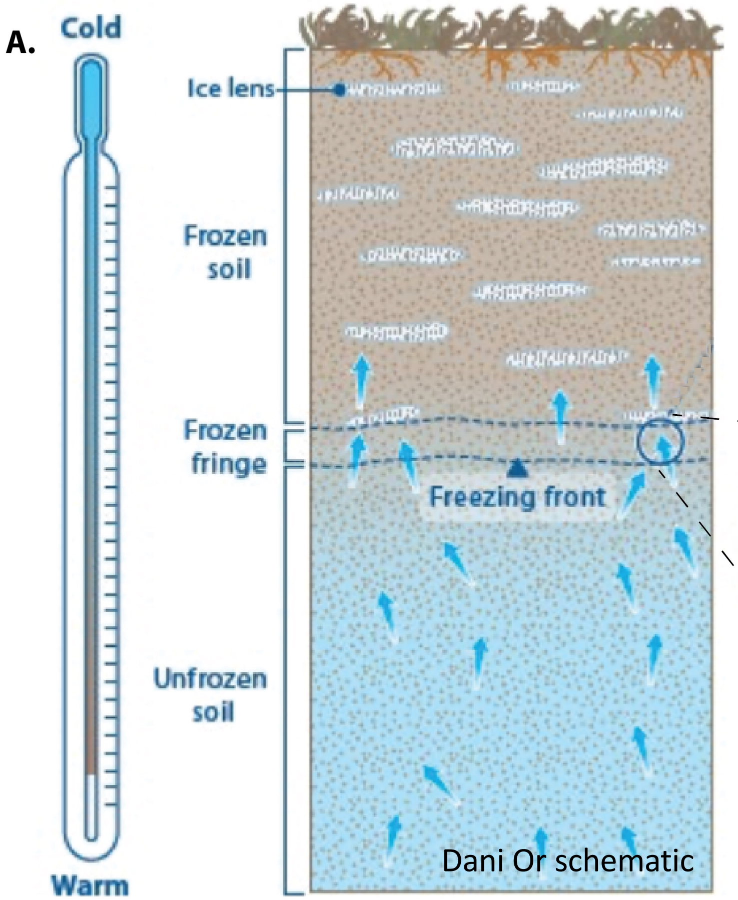

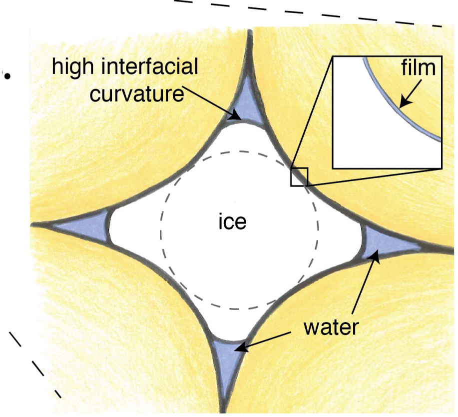

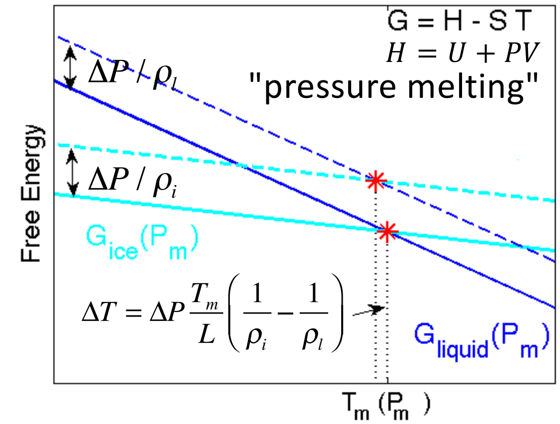

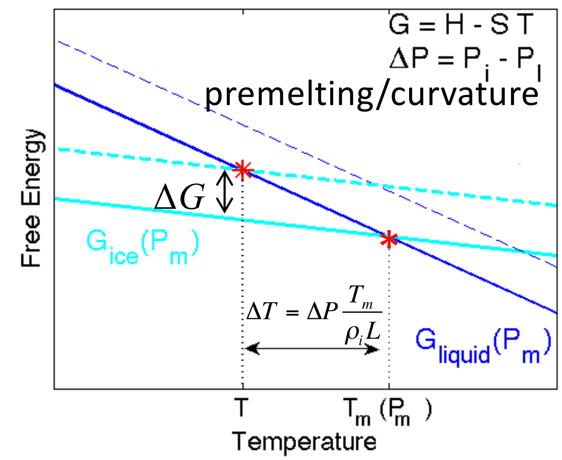

Recall: Along an ice–liquid interface where the ice pressure exceeds the liquid pressure, phase equilibrium is shifted to colder temperatures. In consequence mobile liquid is retained when $T < T_m$ in soils and migrates to colder temperatures where it supplies ice lens growth.

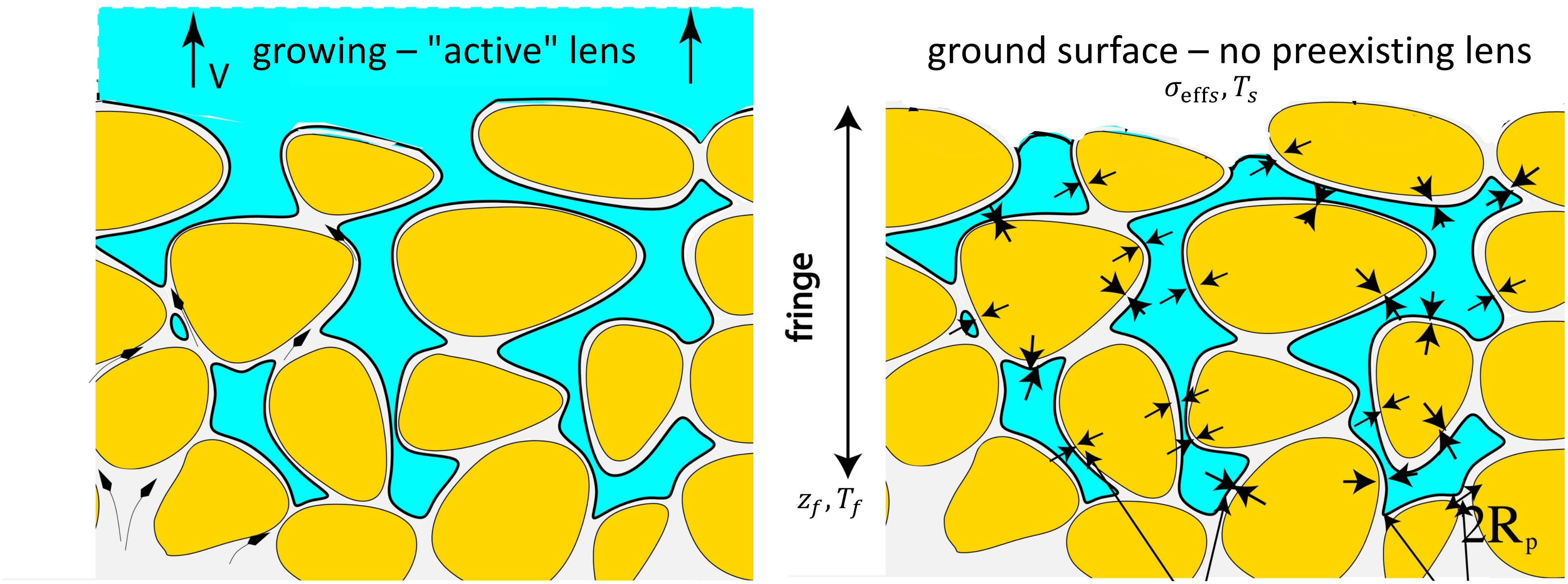

The hydrodynamic pressure adjusts to satisfy the force balance and set the heave rate V, which influences whether and where particles are unloaded in the fringe beneath.

When no preexisting lens is present and the liquid pressure is hydrostatic, a 1st lens can be initiated with the unloading of particle contacts where

$$\sigma_{\text{effs}} + (\rho_B - \rho_l) g \Delta z = \int_z^{z_f} \Pi \, d\Gamma \approx \frac{\rho L}{T_m} n \left[(1 - S_l)(T_m - T) - \int_T^{T_f} (1 - S_l) \, \mathrm{d}T \right]$$

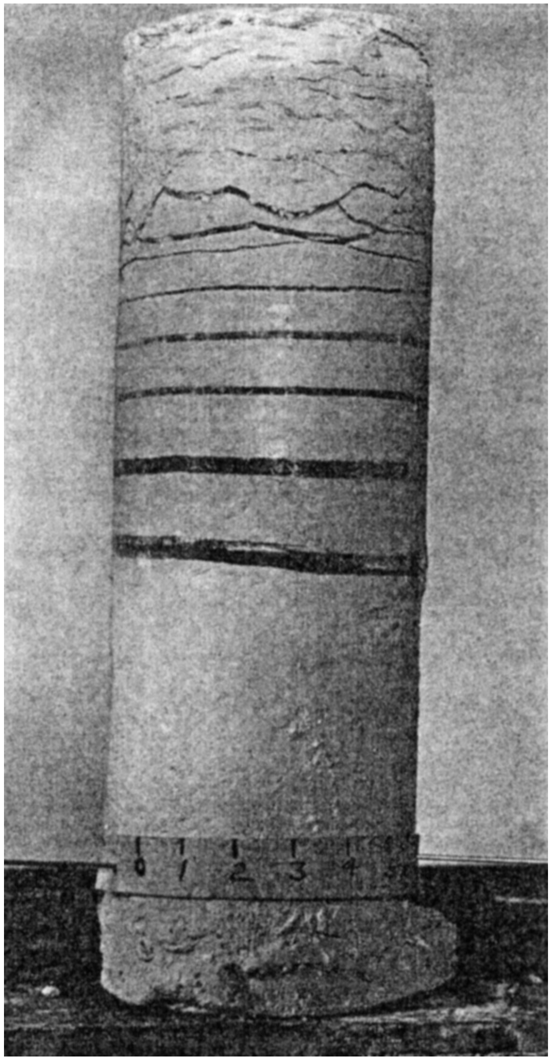

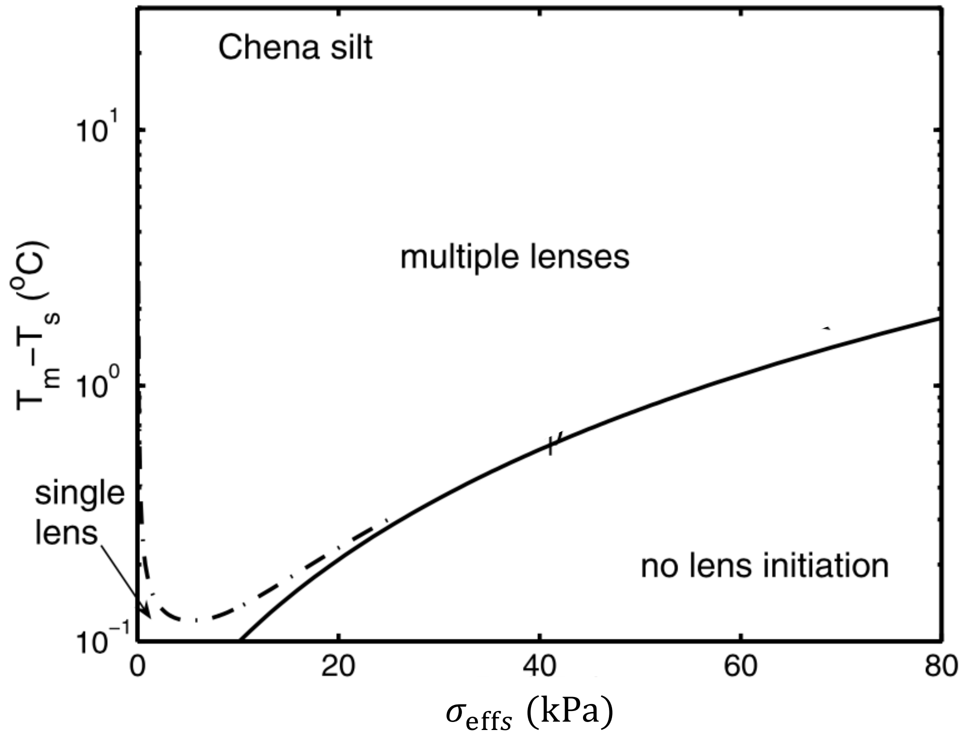

Qualitatively different behavior is expected under different mechanical and thermal forcing (i.e. $\sigma_{\mathrm{eff}s}$ and T_s), with regime boundaries, heave rates, and growth patterns dependent on soil constitutive behavior (i.e S_l and k).

Evolution (freezing or melting) from a pre-existing lens (e.g. needle ice, pingo, glacier).

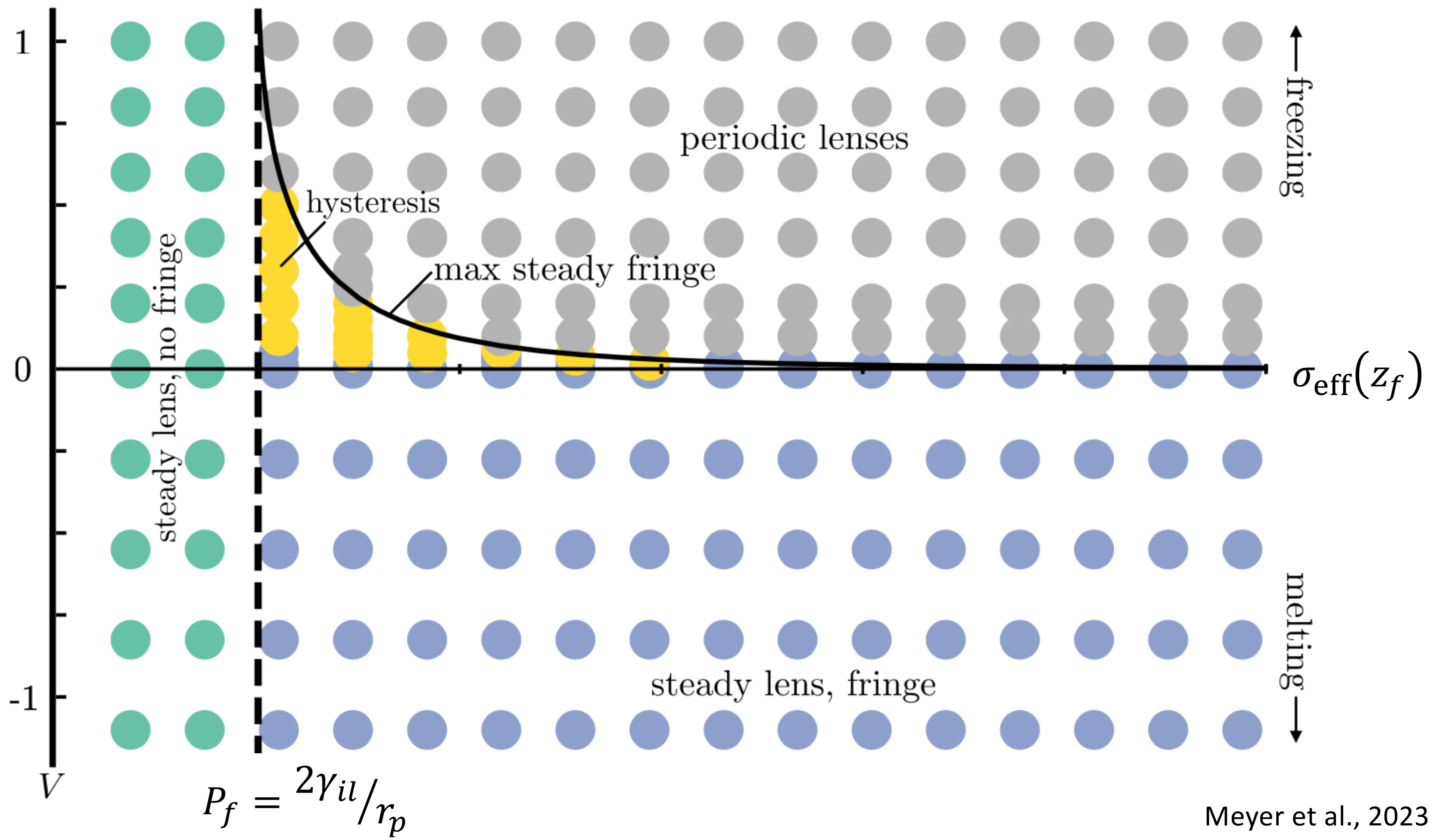

Meyer et al., 2023

Evolution (freezing or melting) from a pre-existing lens (e.g. needle ice, pingo, glacier).

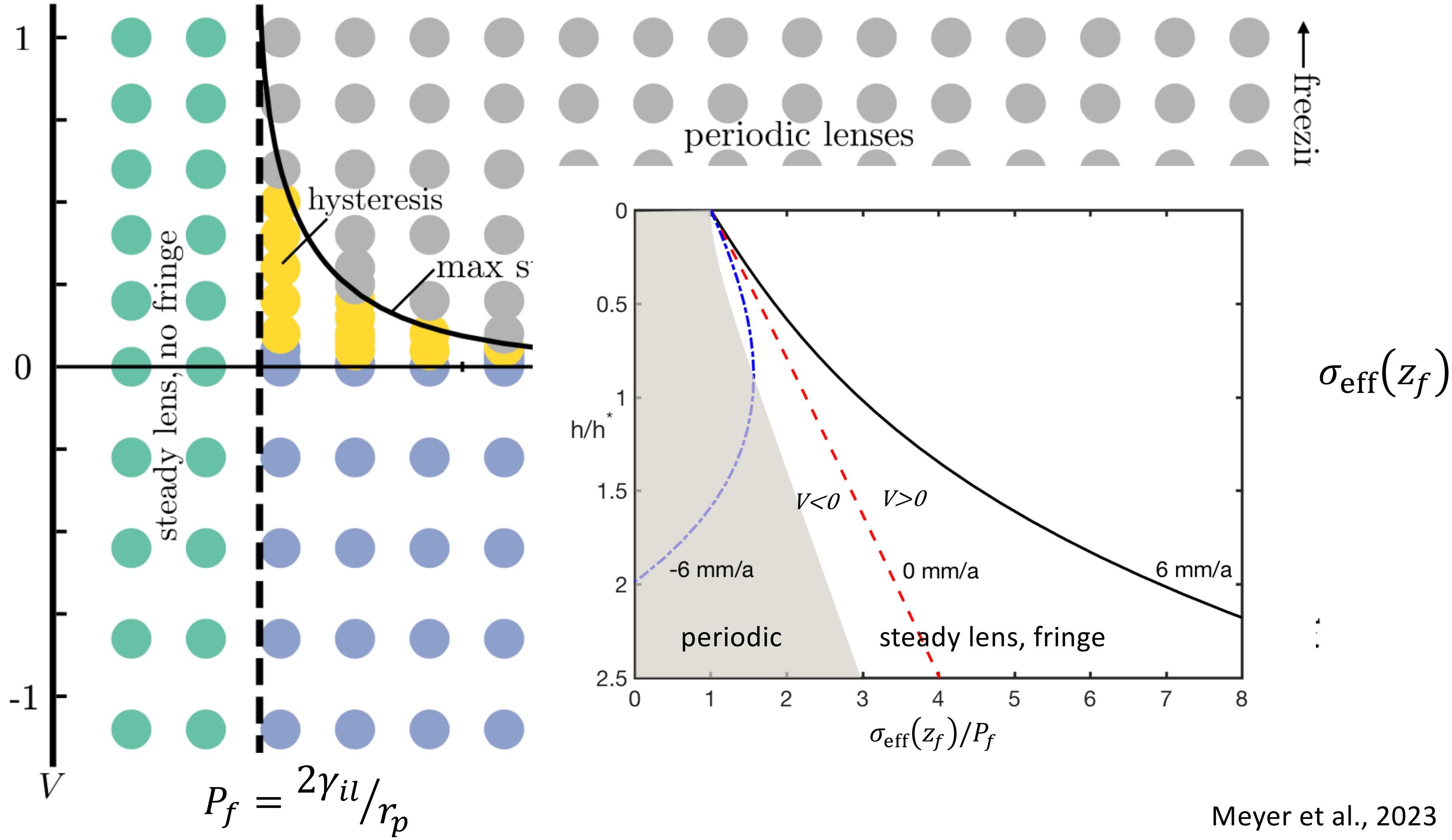

Meyer et al., 2023

Thawing presents its own challenges, with excess water and frozen drainage pathways.

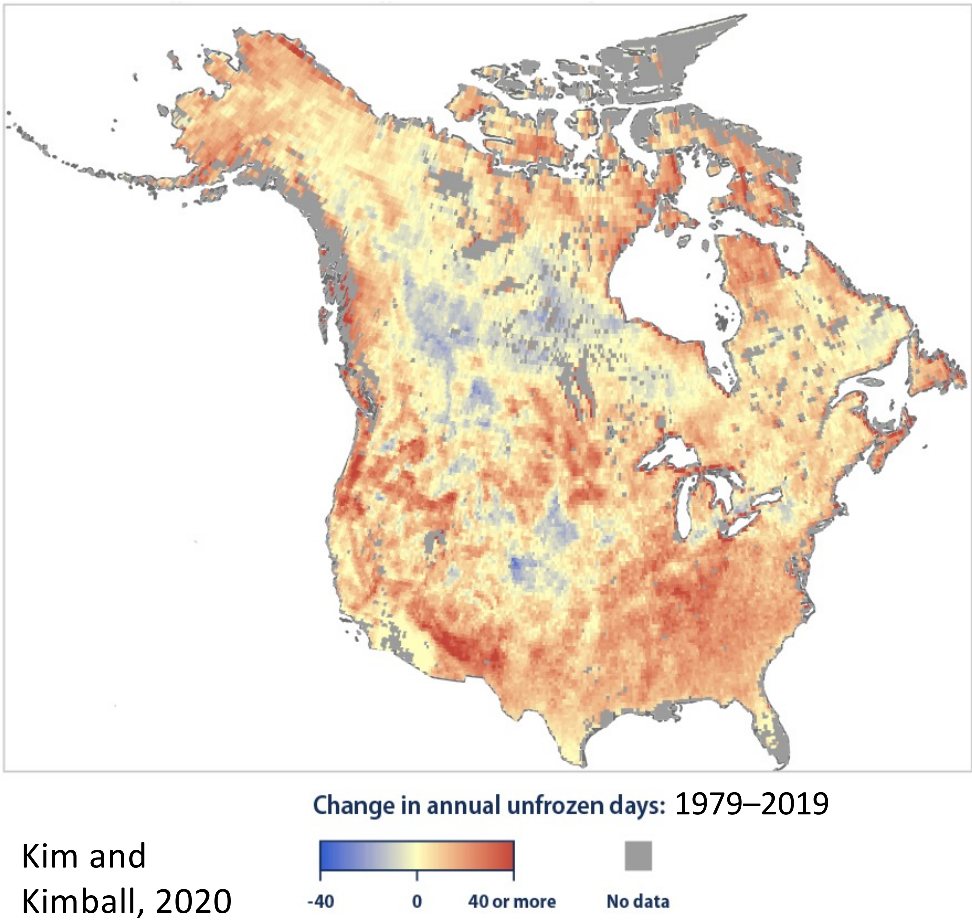

Kim and Kimball, 2020

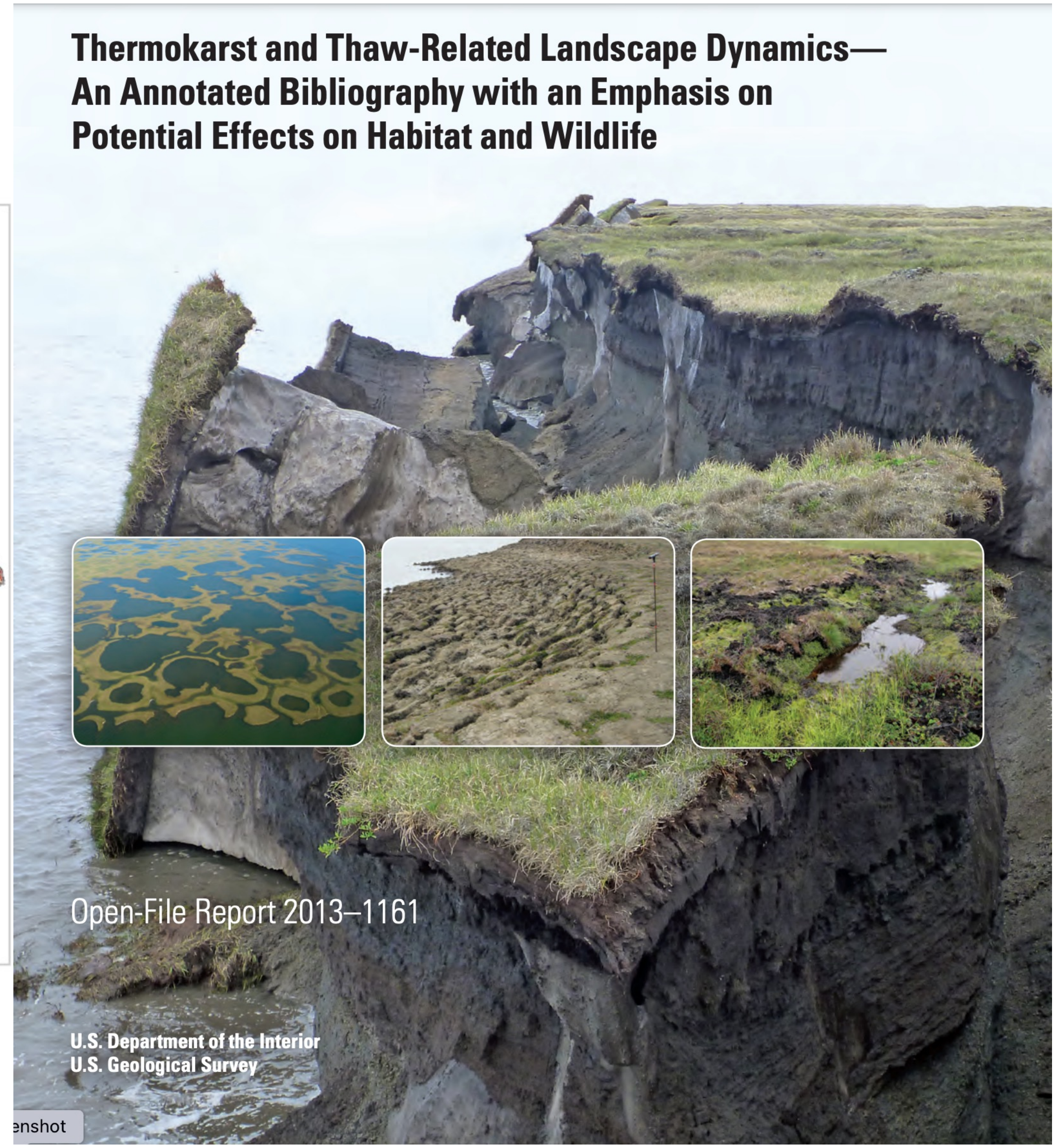

Average annual number of days with freezing conditions at the ground surface inferred from satellite microwave brightness from 1979-2014 by Kim et al., 2017.

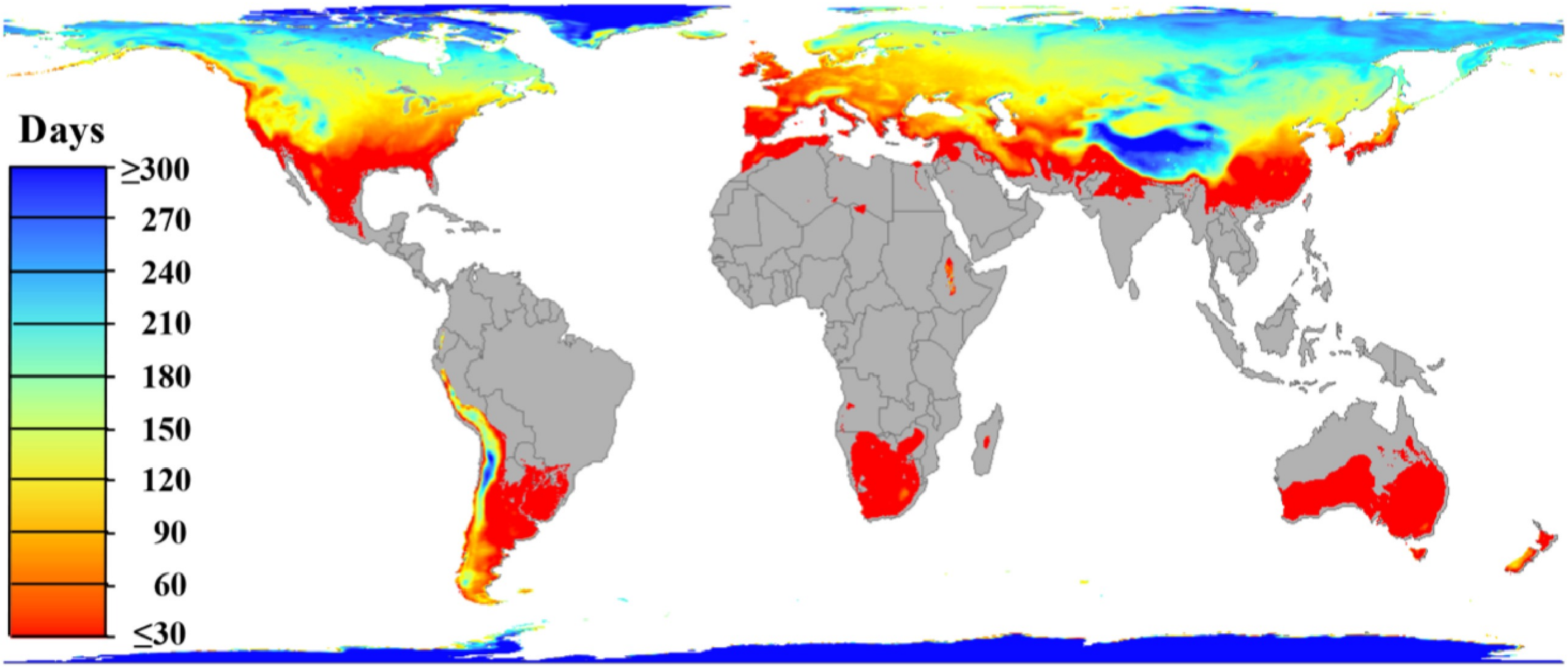

Frost action is limited to needle ice growth in locations with infrequent freezing.
Where frequent freezing occurs, significant frost damage is often restricted to fall and spring.
Persistent, active ice–water–sediment interactions at modest effective stress occur subglacially.

Could subglacial ice–water–sediment interactions be societally important, as well as interesting?

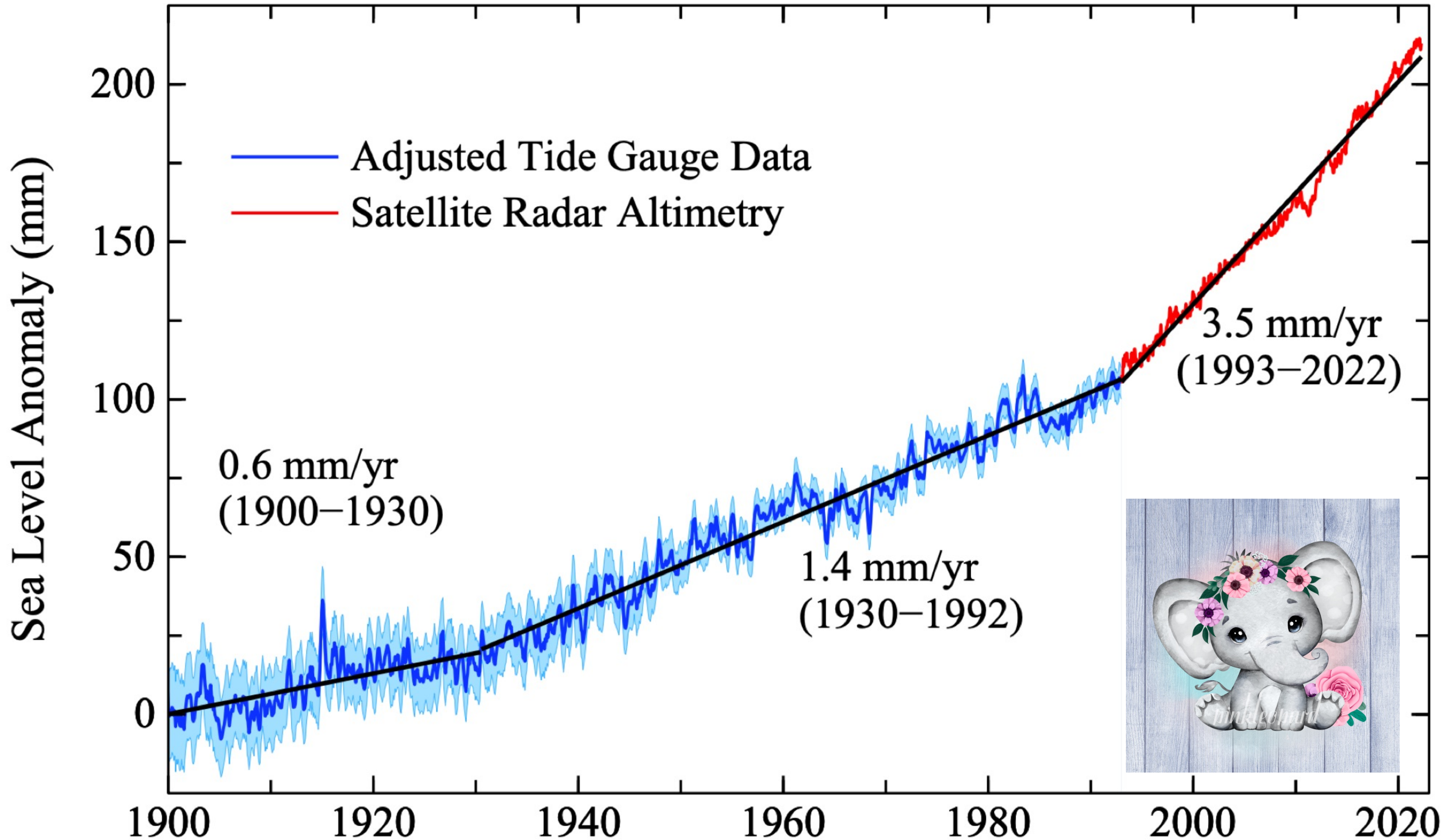

Church and White, 2011

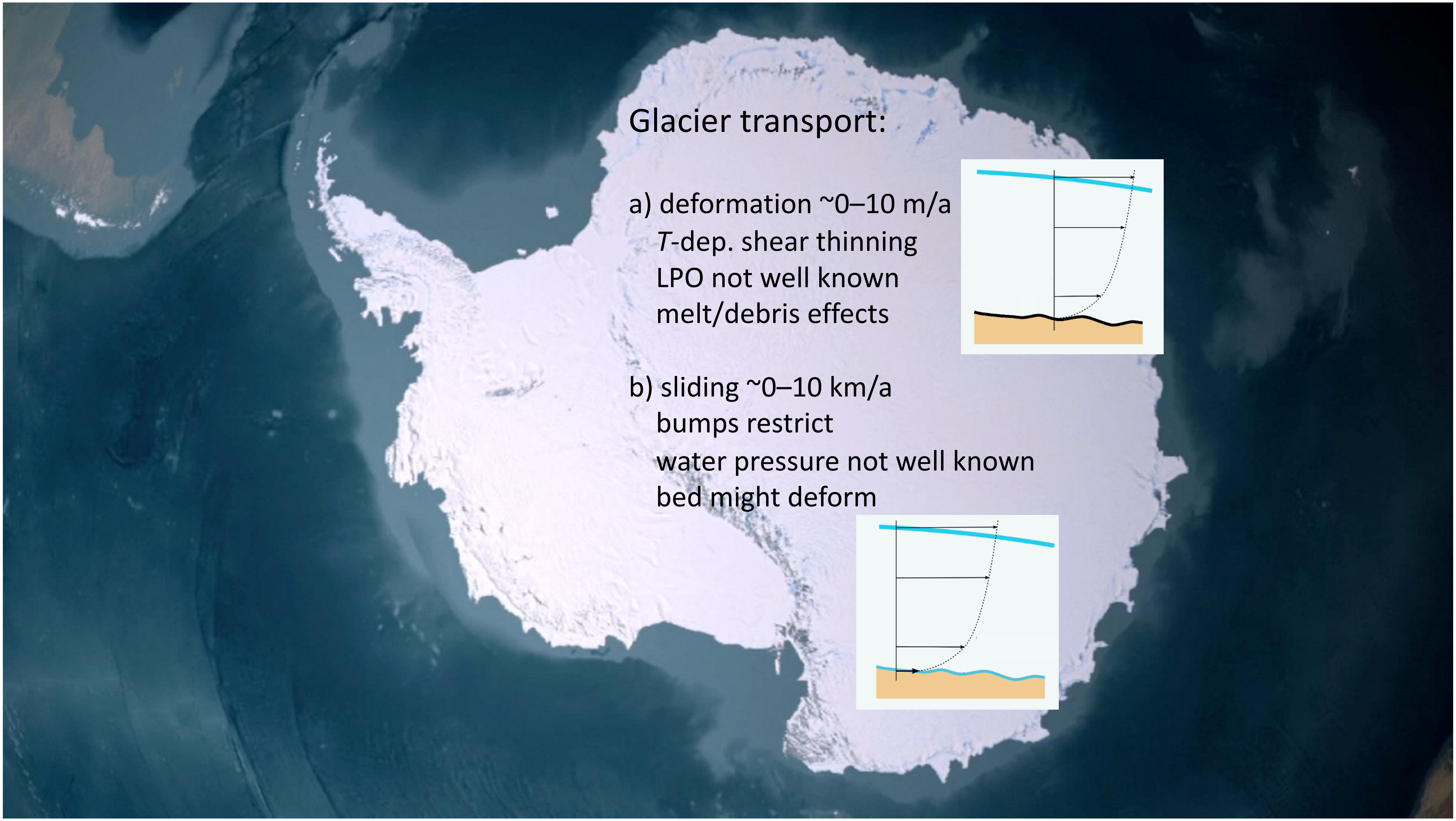

Glacier transport:

a) deformation ~0–10 m/a
T-dep. shear thinning
LPO not well known
melt/debris effects

b) sliding ~0–10 km/a
bumps restrict
water pressure not well known
bed might deform

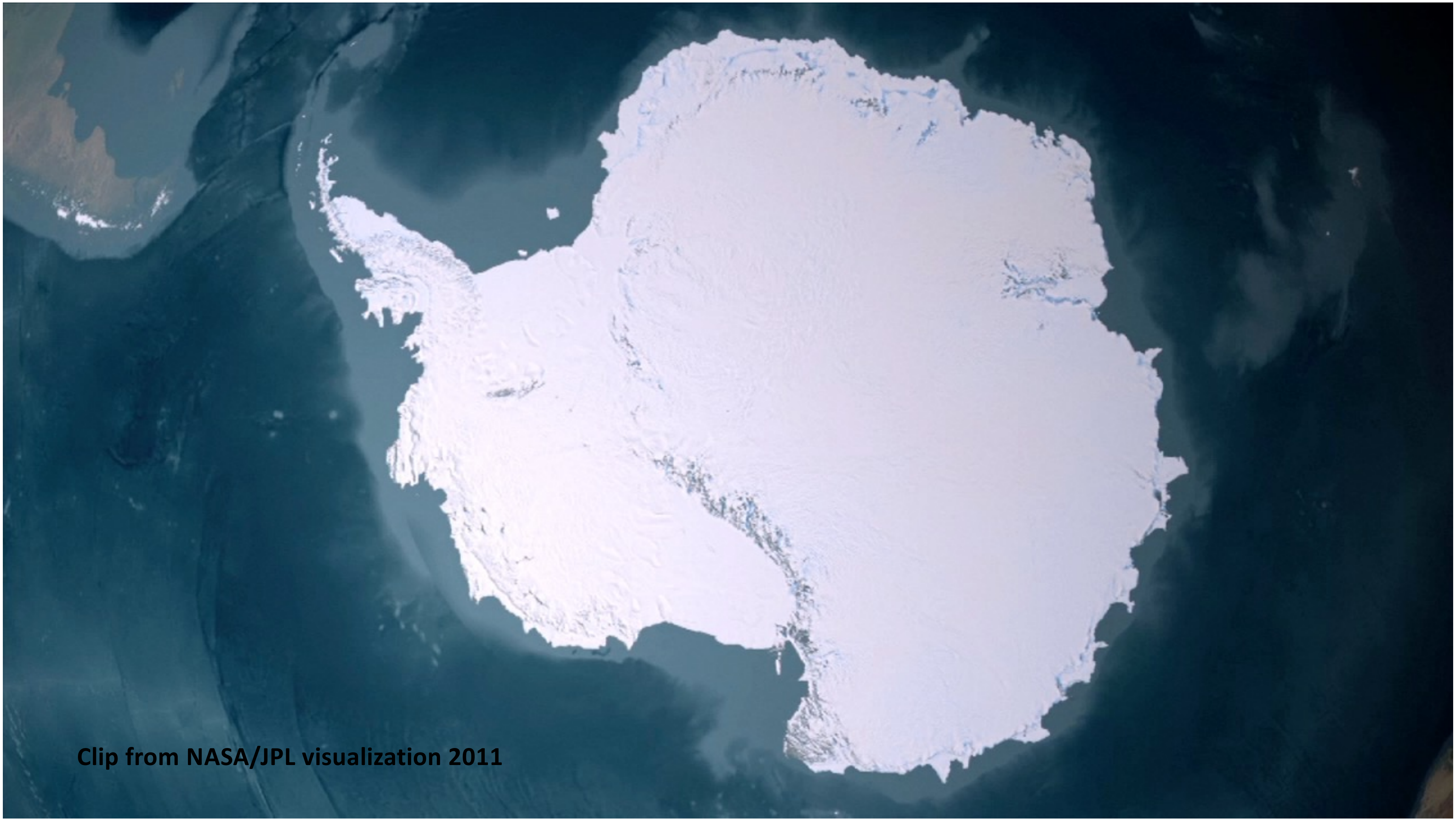

Clip from NASA/JPL visualization 2011

Current simulations do not provide consistent forecasts of long-term glacier dynamics.

Major Uncertainties:

Human behavior

Atmospheric forcing

Ice–ocean interactions

Ice–bed coupling

Ice rheology

Numerics

Note: despite problems, for sea level rise during a typical life-span, uncertainty over ice dynamics is not the dominant concern.

Volume change in m Sea Level Equivalent (SLE) with ice shelves removed.

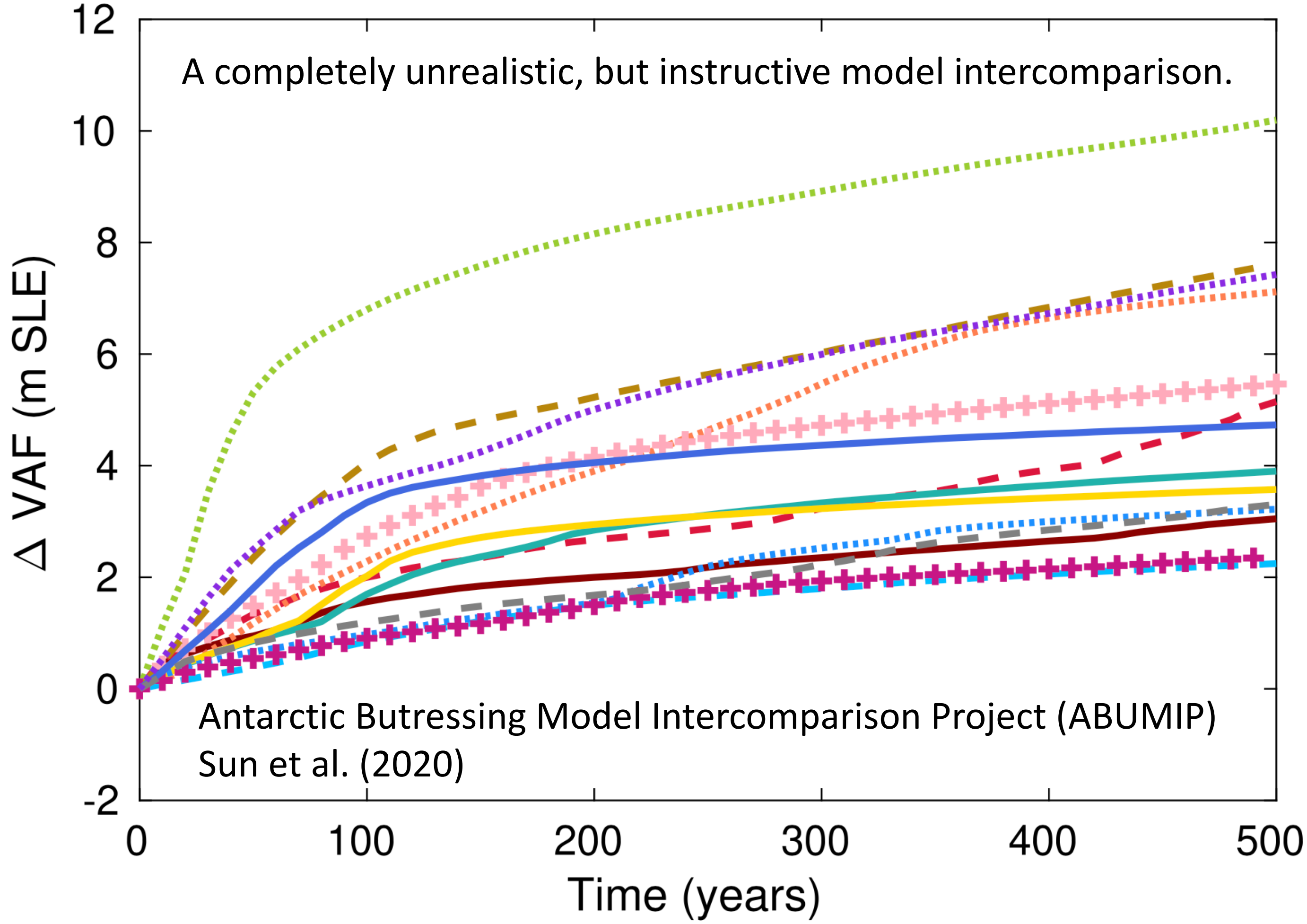

Simulated ice–bed coupling is not as well-grounded in physics as one might like.

Most ice discharge occurs through narrow, fast-flowing streams.

Current ice sheet simulations rely upon an invariant, heterogeneous slipperiness index.

They are designed to *extrapolate* from current observations into the future.

Sliding velocity v_b is treated here as proportional to basal shear stress τ_b.

$$\alpha^2 v_b = -\tau_b$$

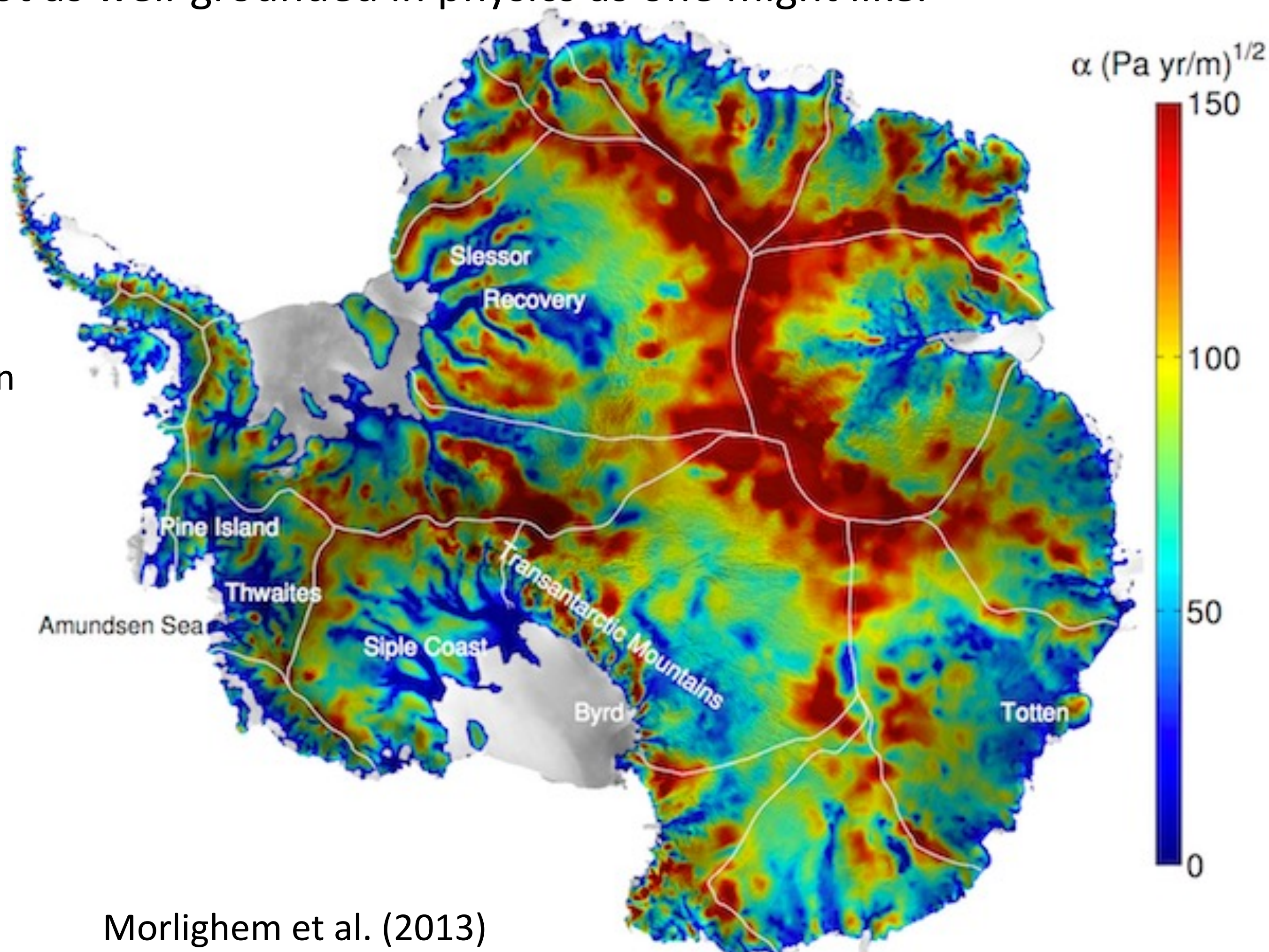

Morlighem et al. (2013)
(inversion using surface velocities; others use elevation)

Abrupt mechanical transitions and transients are not captured.

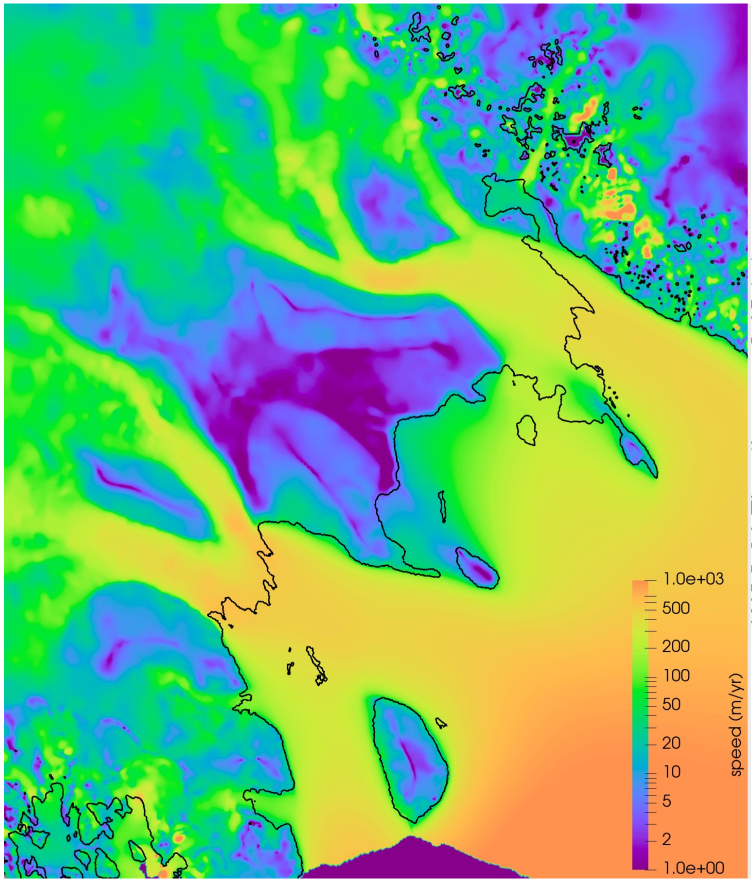

Hoffman et al. (2018)

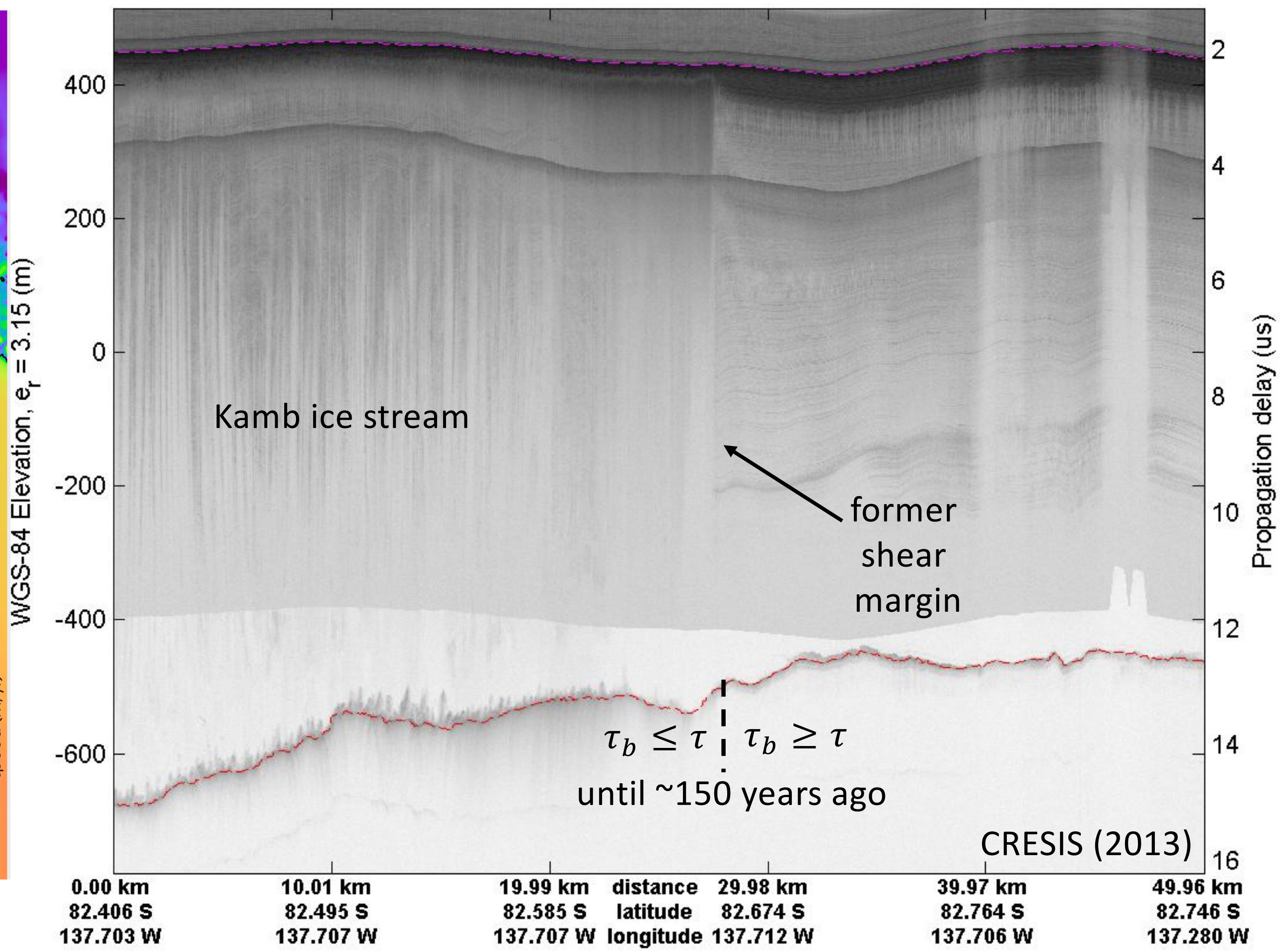

Warm (possibly wet, *Hunter et al. 2019)* ice in narrow shear margins is aliased to the coarse slipperiness field.

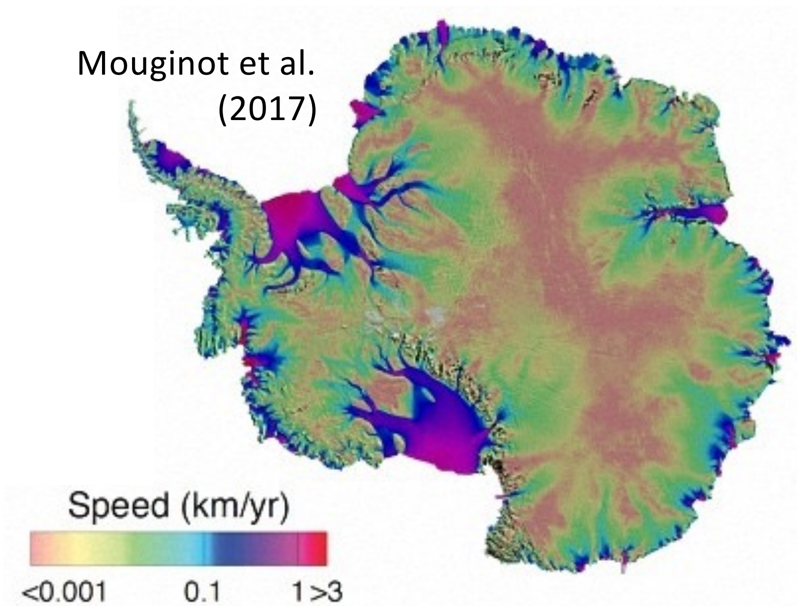

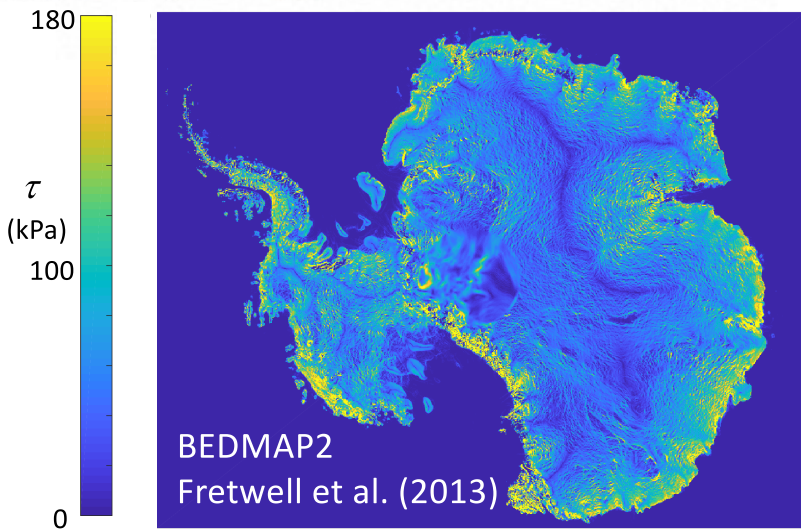

Observations:

– much (> 50%) of the bed is at the melting point (i.e. can slide)
– over km^2 areas basal shear stress τ_b matches driving stress τ
– median τ is about 60–70 kPa
– driving stress isn't spatially correlated with ice speed v

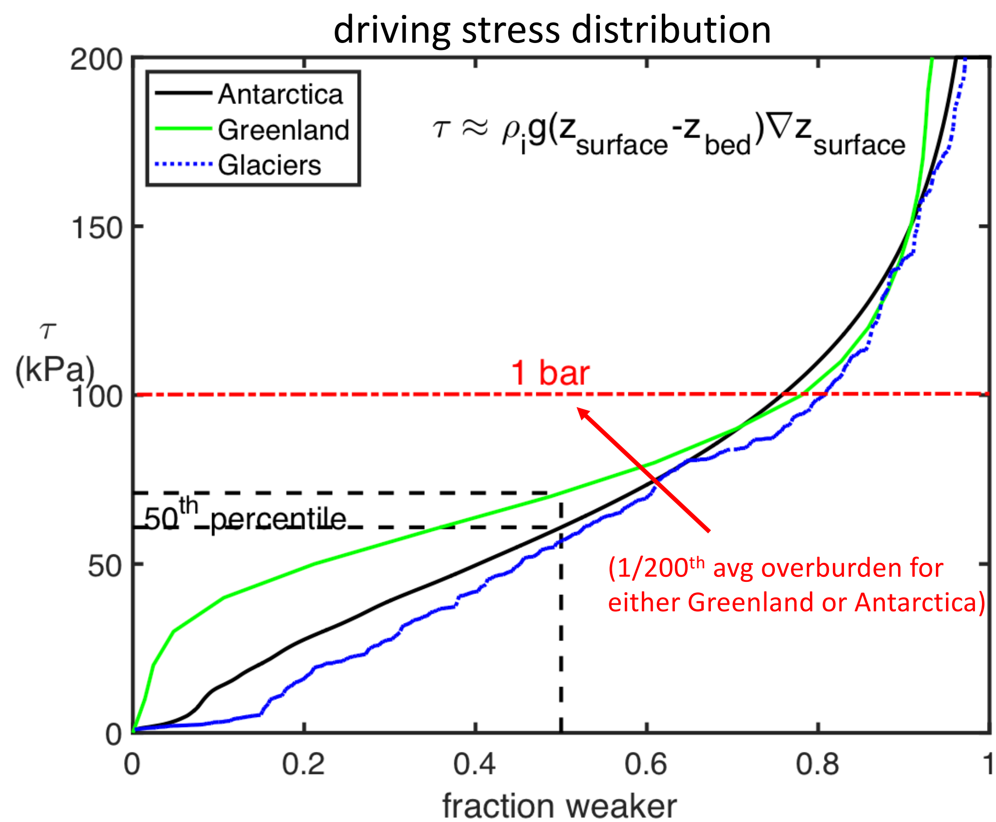

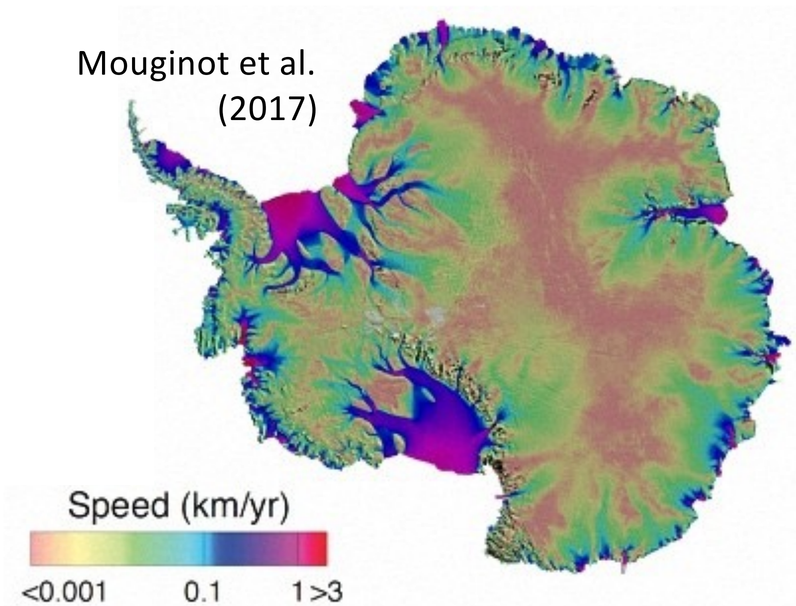

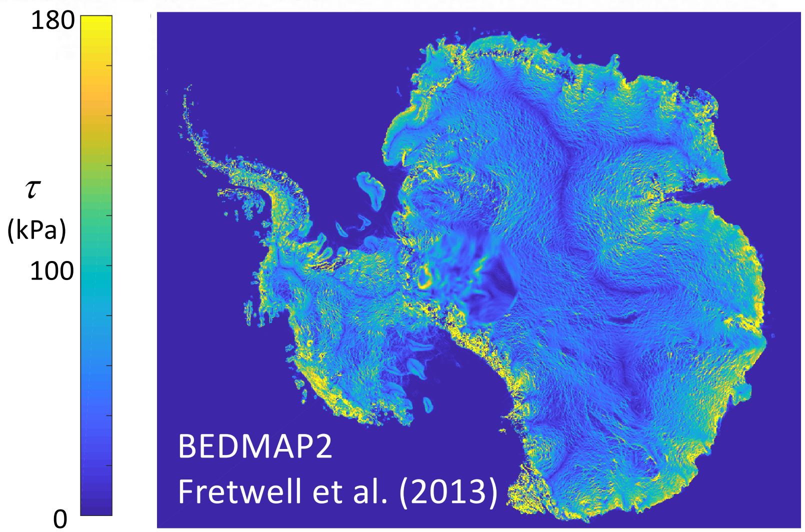

Observations:

– much (> 50%) of the bed is at the melting point (i.e. can slide)

– over km^2 areas basal shear stress τ_b matches driving stress τ

– median τ is about 60–70 kPa

– driving stress isn't spatially correlated with ice speed v

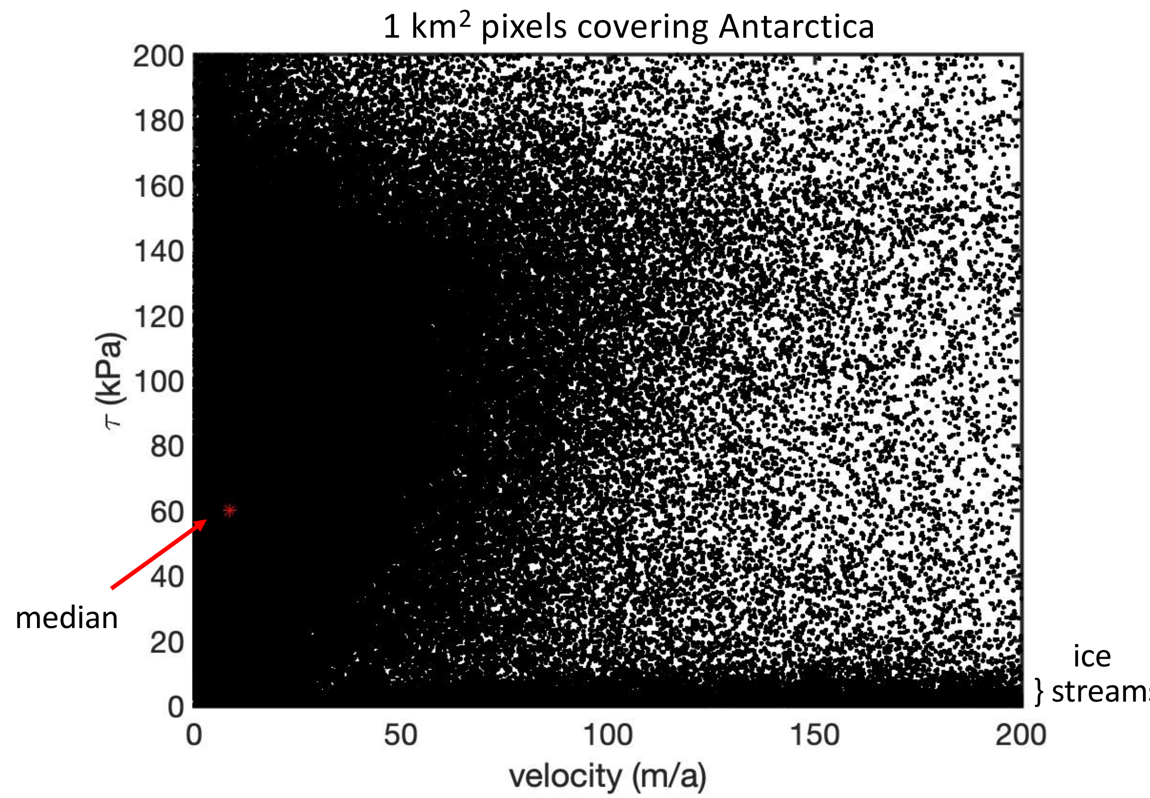

Sliding observations from experiments:

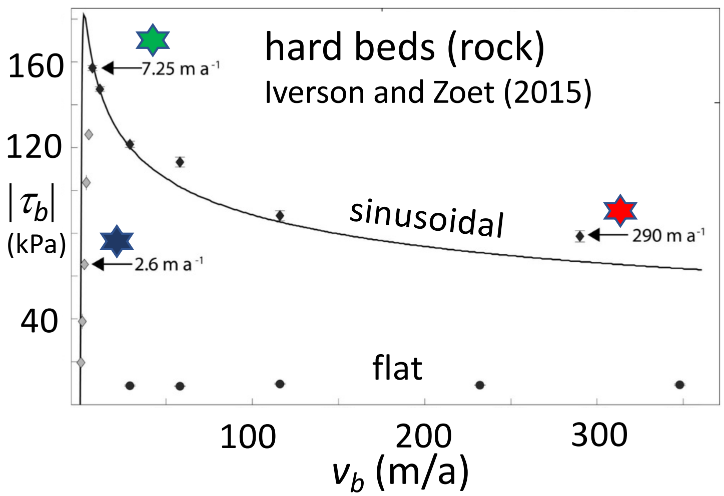

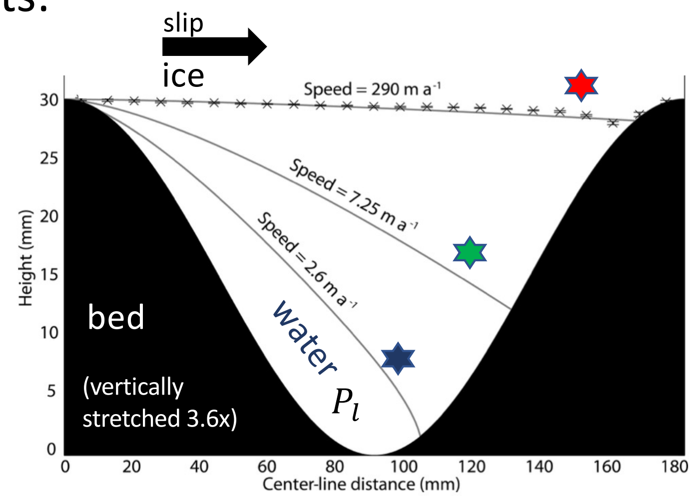

Low speeds:
rate-strengthening
e.g. $\alpha^2 v_b = -\tau_b$

High speeds:
rate-weakening
or plastic

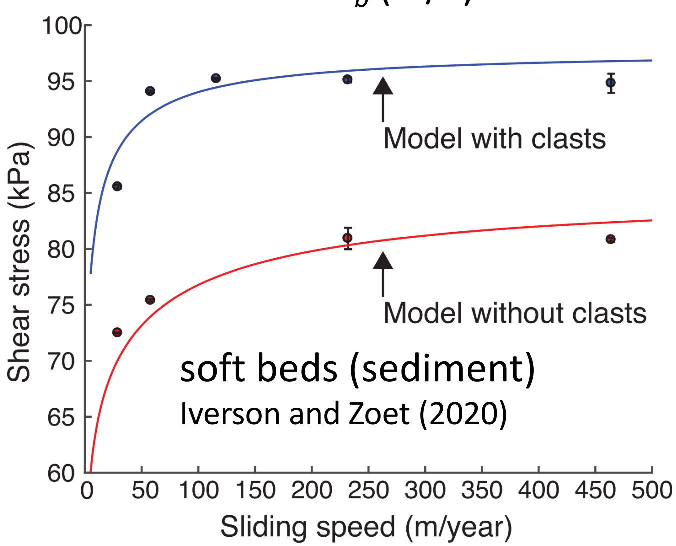

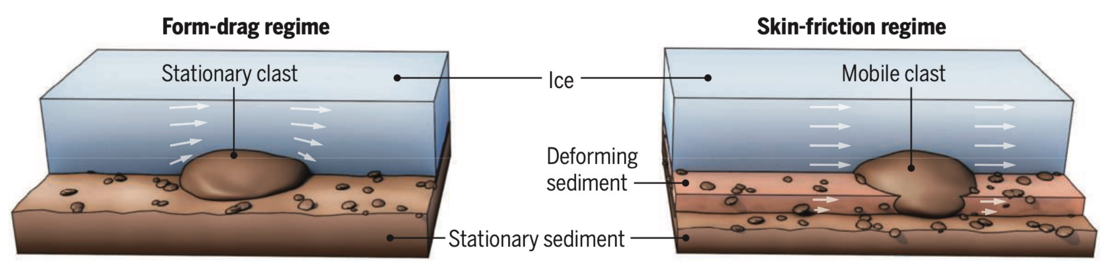

Minchew and Joughin (2020)

Water pressure P_l and phase behavior affect τ_b.

Subglacial drainage systems regulate P_l.

Relevant stresses:

$P_l = -\sigma_{\mathrm{nn}}$ along conduits.

Creep closure parameterizations use

$$N = \rho_i g \bar{H} - P_l.$$

Away from conduits, coupling depends on

$$\sigma_{\mathrm{eff}} = -\sigma_{\mathrm{nn}} - P_l.$$

conduits

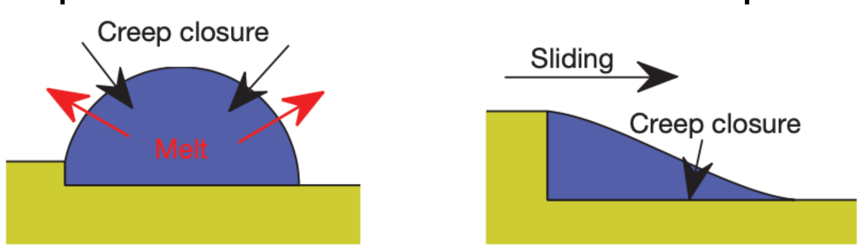

Schoof (2010)

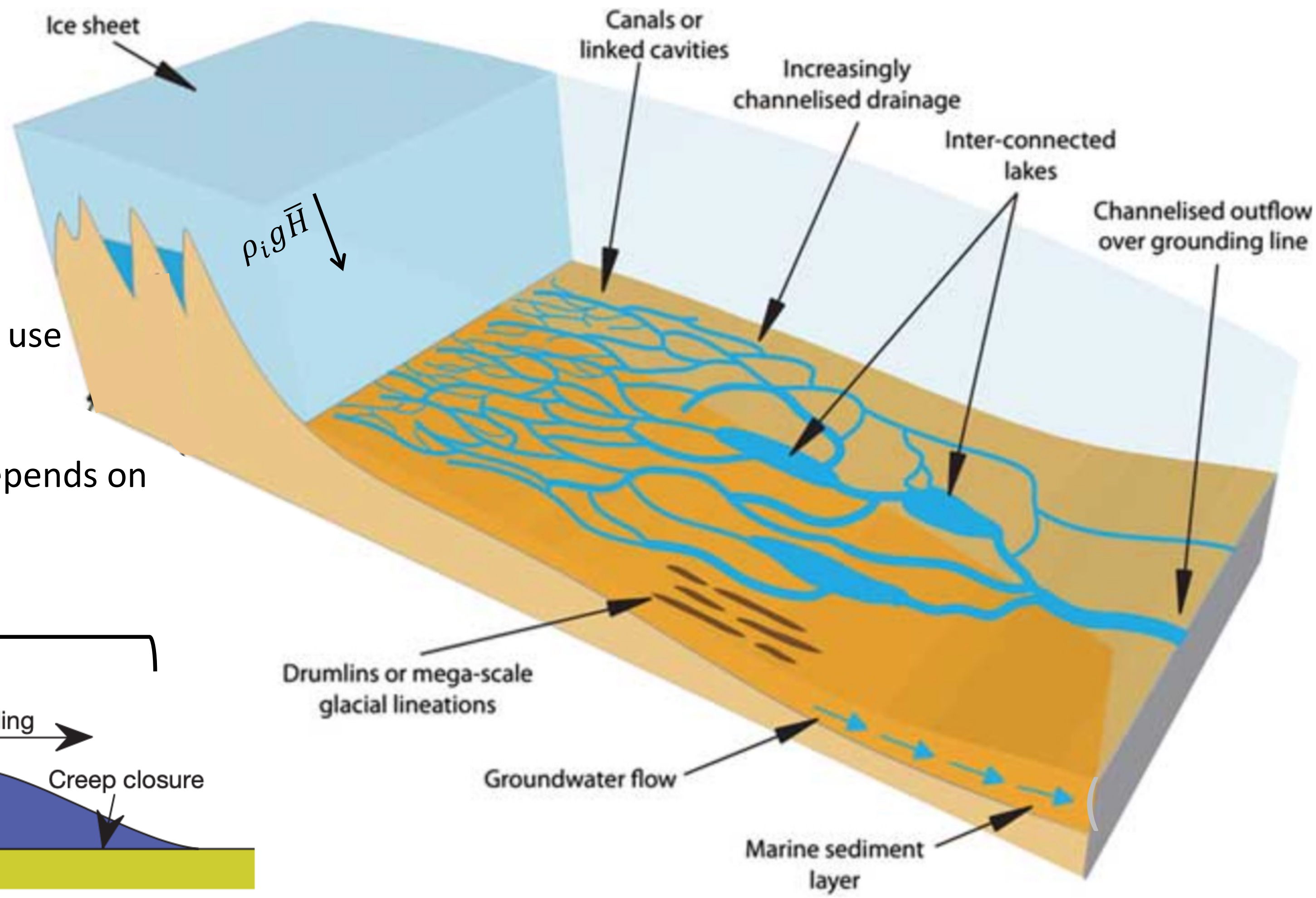

Ashmore and Bingham (2014)

Ice–liquid equilibrium depends on both P_l and $-\sigma_{\mathrm{nn}}$.

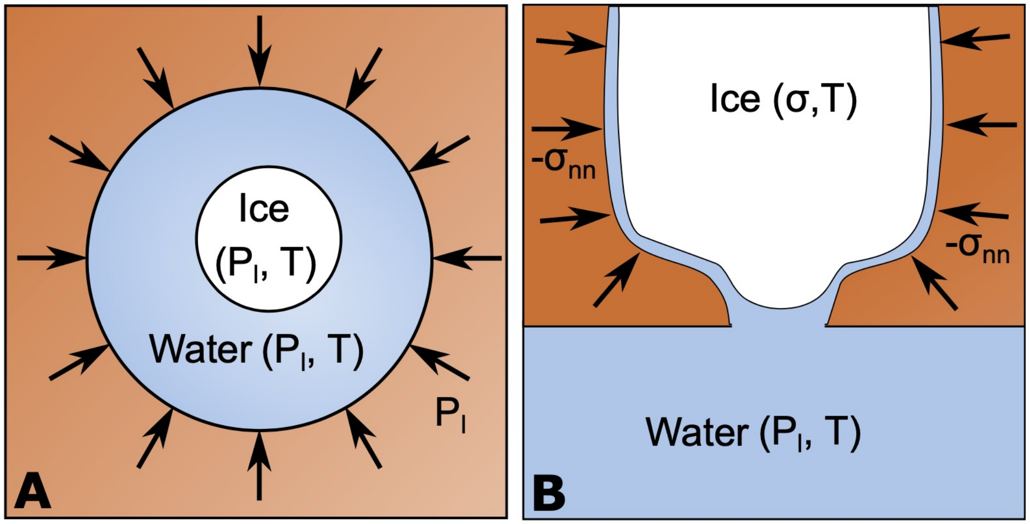

Case (i): Ice growth in a closed space

Case (ii): Ice growth in an open pore

Linear Clapeyron equation (pure water, no solutes):

$$T \approx T_m \left(1 + \frac{\sigma_{\mathrm{nn}} + P_m}{\rho_s L} + \frac{P_l - P_m}{\rho_l L}\right)$$
$$= T_m \left[1 - \frac{\sigma_{\mathrm{eff}}}{\rho_s L} - \frac{P_l - P_m}{\rho_s \rho_l L}(\rho_l - \rho_s)\right]$$

Areas with $-\sigma_{\mathrm{nn}} = P_l$ are required and areas with $-\sigma_{\mathrm{nn}} > P_l$ are expected.

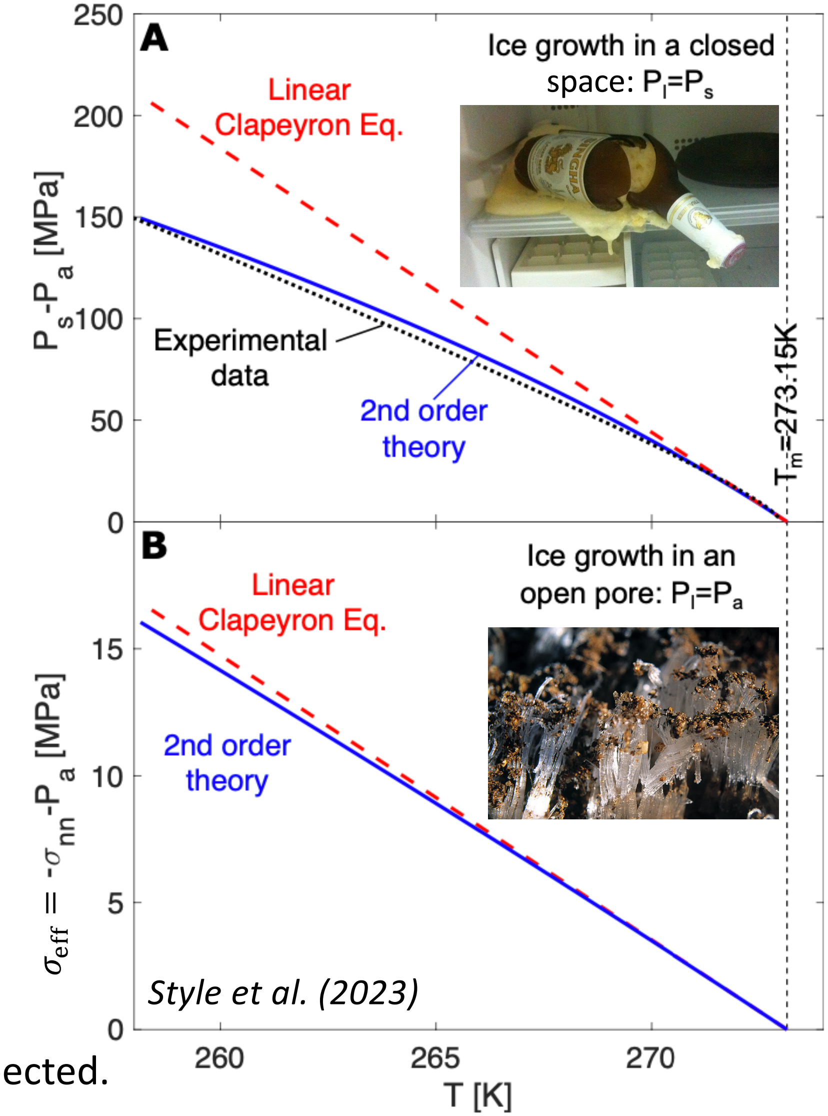

"Free(ish) slip" at the smallest scales:

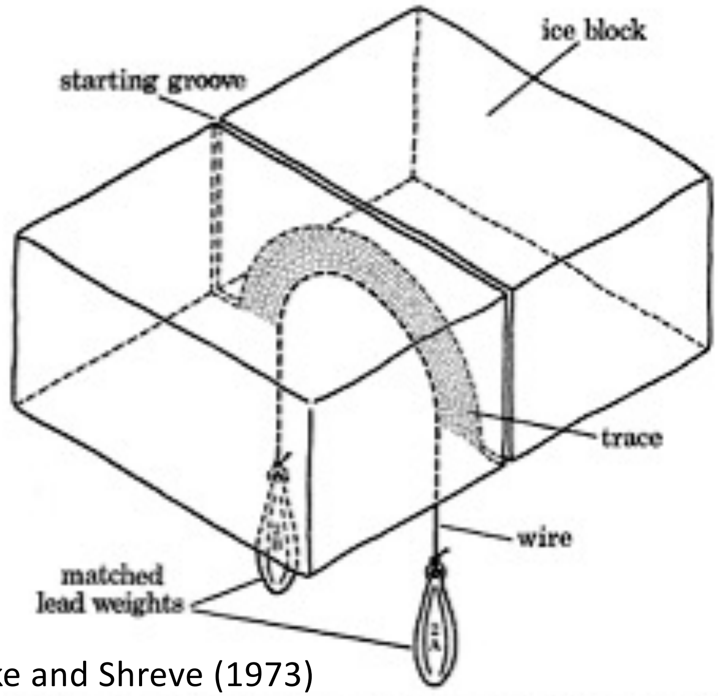

Drake and Shreve (1973)

Regelation enables motion past small bumps by melting on the upstream side and refreezing on the downstream side.

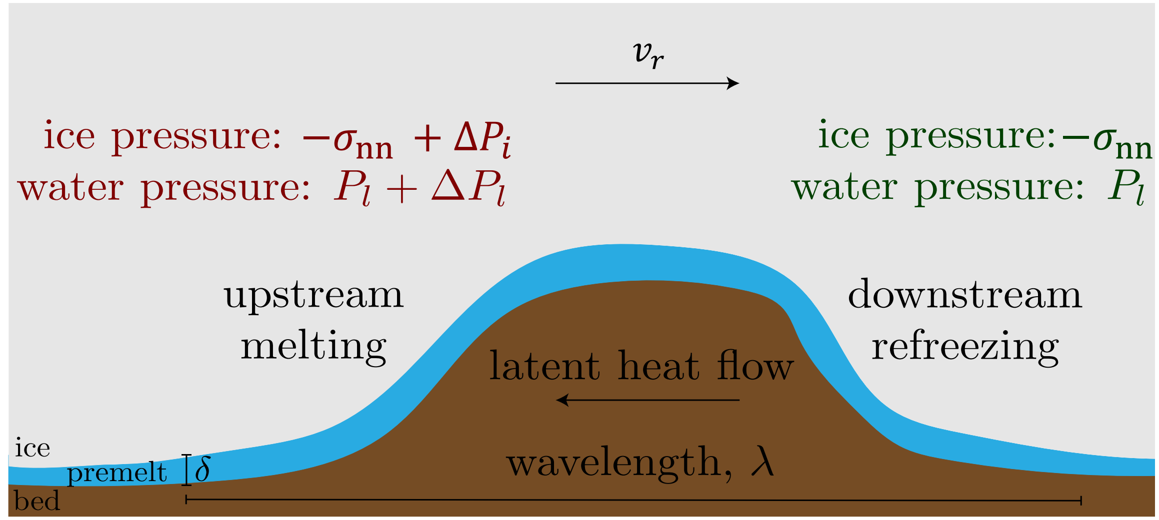

Conduction of latent heat limits regelation rate:

$$\rho_i L v_r \sim -K\,\frac{\Delta T}{\lambda/2}\ .$$

Allowing for differences between $-\sigma_{nn}$ and P_l leads to:

$$\rho_i L v_r \sim \frac{2KT_m}{\rho_i L \lambda}\Delta P_i\left(1-\frac{\rho_i \Delta P_l}{\rho_l \Delta P_i}\right)\ .$$

For given ΔP_i:

$$v_r|_{\Delta P_l \ll \Delta P_i} \approx 12\ v_r|_{\Delta P_l = \Delta P_i}\ .$$

($\Delta\sigma_{\rm eff} > 0$, *open*) ($\Delta\sigma_{\rm eff} = 0$, *closed*)

Glaciology's effective stress problem: σ_{eff} vs. N

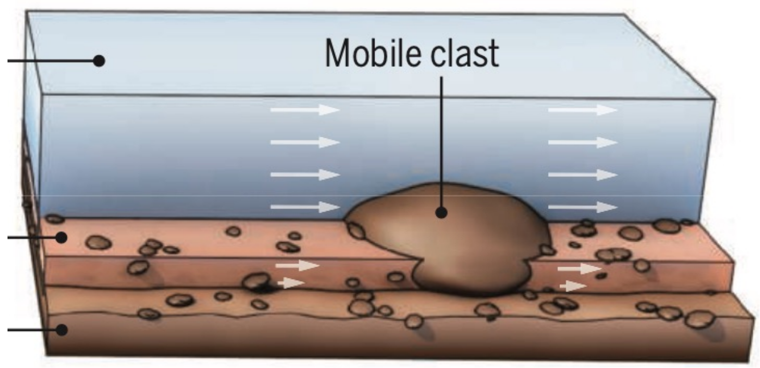

Subglacial mechanical coupling depends on

$$\sigma_{\text{eff}} = -\sigma_{\text{nn}} - P_l.$$

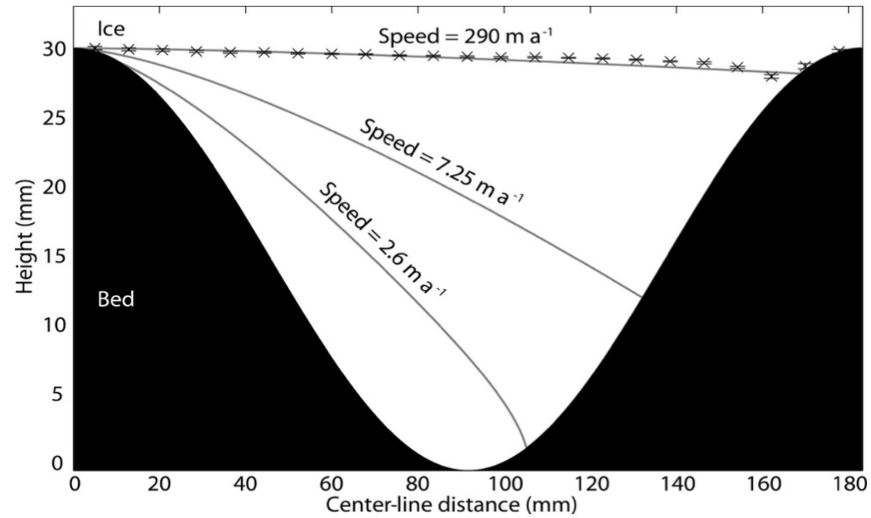

Subglacial drainage models depend on

$$N = \rho_i g \bar{H} - P_l.$$

Castleguard

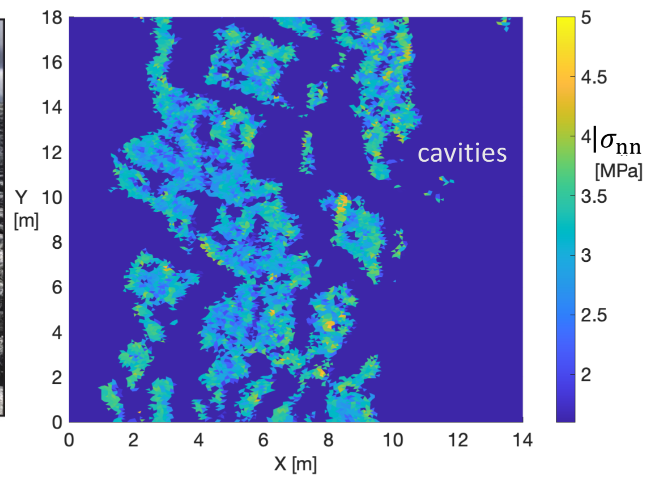

Helanow et al (2021)

Ice thickness $\bar{H}$ and P_l can be measured, but $-\sigma_{\text{nn}}$ generally must be calculated (see left).

Advanced coupled treatments often assume $-\sigma_{\text{nn}} = P_l$ (i.e. $\sigma_{\text{eff}} = 0$) everywhere.

To what extent are basal ice–water systems open (i.e. $\sigma_{\text{eff}} > 0$) or closed (i.e. $\sigma_{\text{eff}} = 0$)?

Evidence for direct ice–bed coupling ($\sigma_{\mathrm{eff}} > 0$) I: seismic

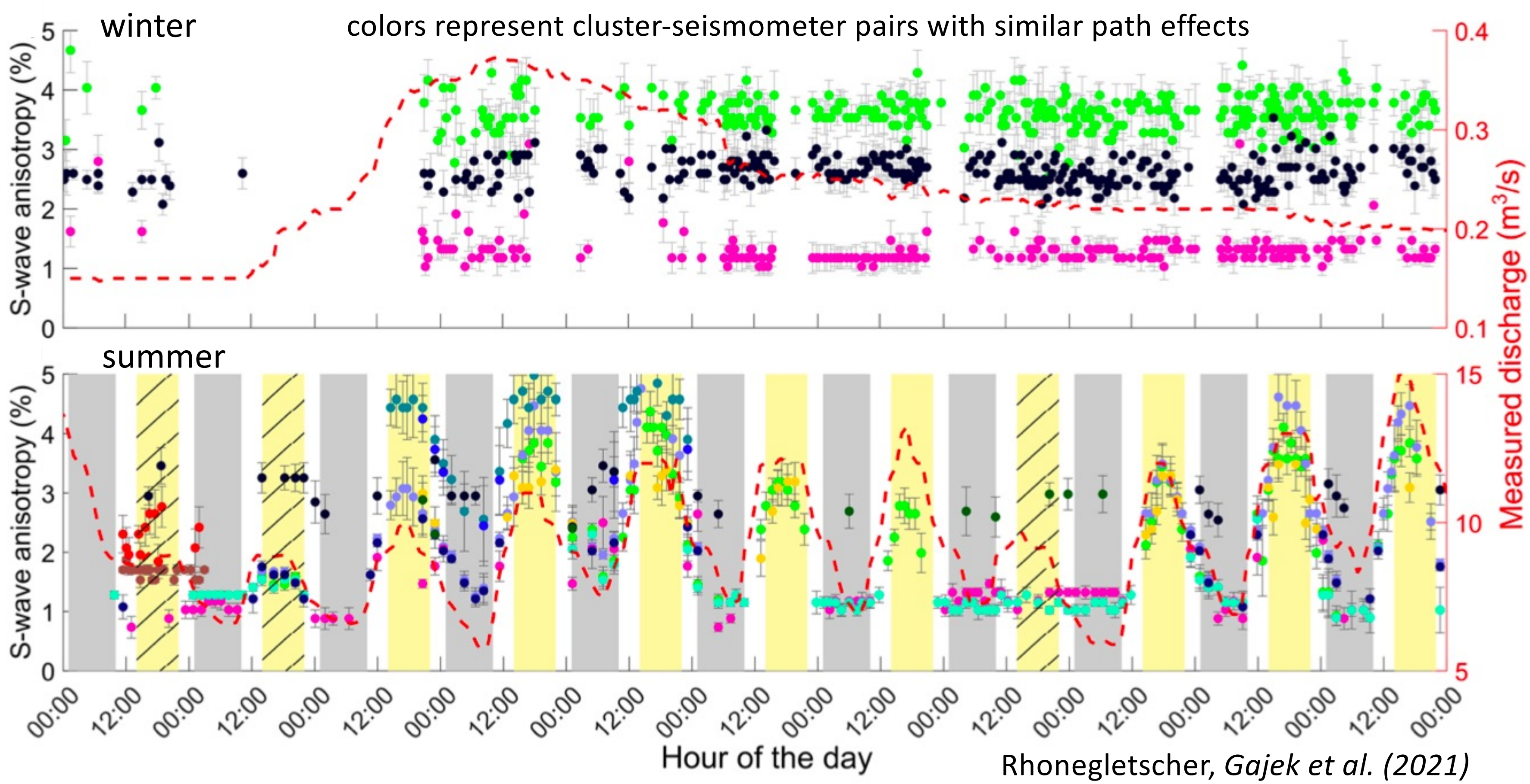

Shear-wave splitting suggests hydraulic fracture of basal ice → $P_l \sim |\sigma_{\min}| < |\sigma_{\mathrm{nn}}|$

Evidence for direct ice–bed coupling ($\sigma_{\text{eff}} > 0$) II: thermodynamic

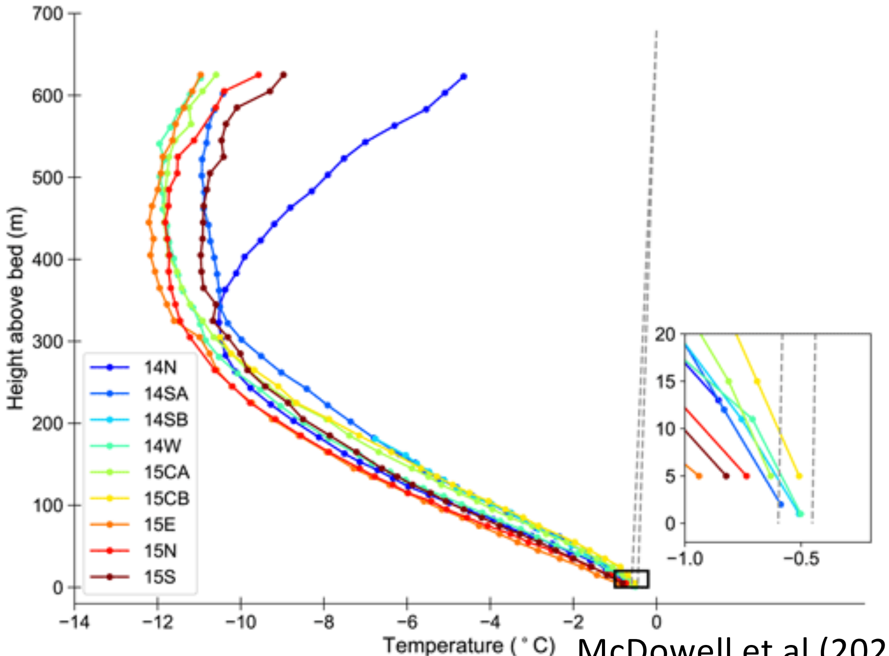

McDowell et al (2021)

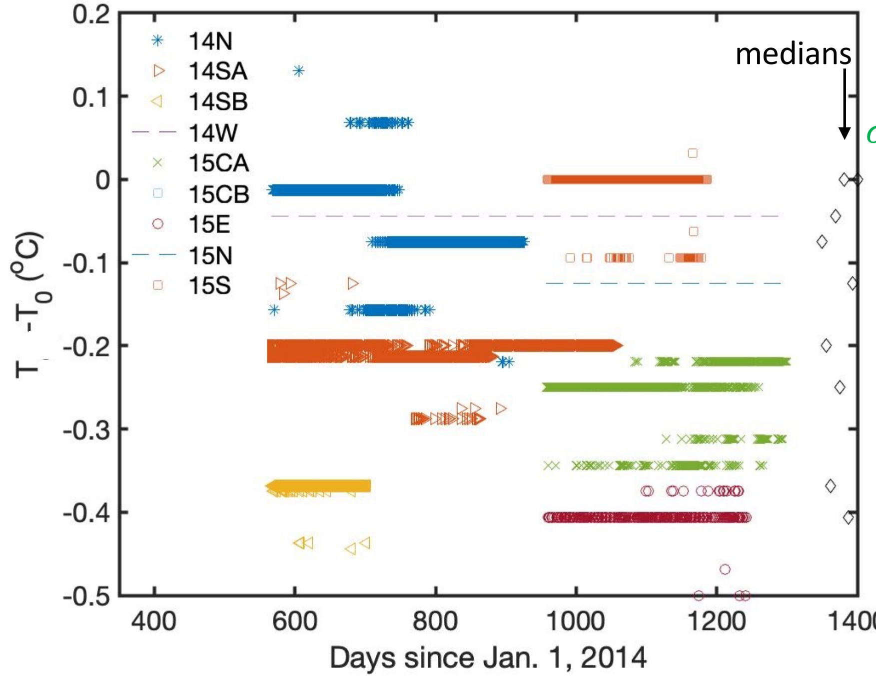

σ_{eff}; $-\sigma_{\text{nn}} - P_0$ (MPa)

0.11; 1.35

0.22; 2.70

0.33; 4.05

0.44; 5.40

Boreholes terminated above Greenland bed.
Thermal evolution suggests crevasse healing.

Basal T below local $T_0(P_0)$ suggests either:

Closed: if $P_l = -\sigma_{\text{nn}}$, then $T - T_0 \approx \frac{T_0}{\rho_s L}\frac{\rho_l - \rho_s}{\rho_l}(-\sigma_{\text{nn}} - P_0)$

Open: if $P_l \approx P_0$, then $T - T_0 \approx \frac{T_0}{\rho_s L}\sigma_{\text{eff}}$

Closed: large, persistent overpressures or

Open: modest σ_{eff}

Evidence for direct ice–bed coupling ($\sigma_{\mathrm{eff}} > 0$) III: hydraulic

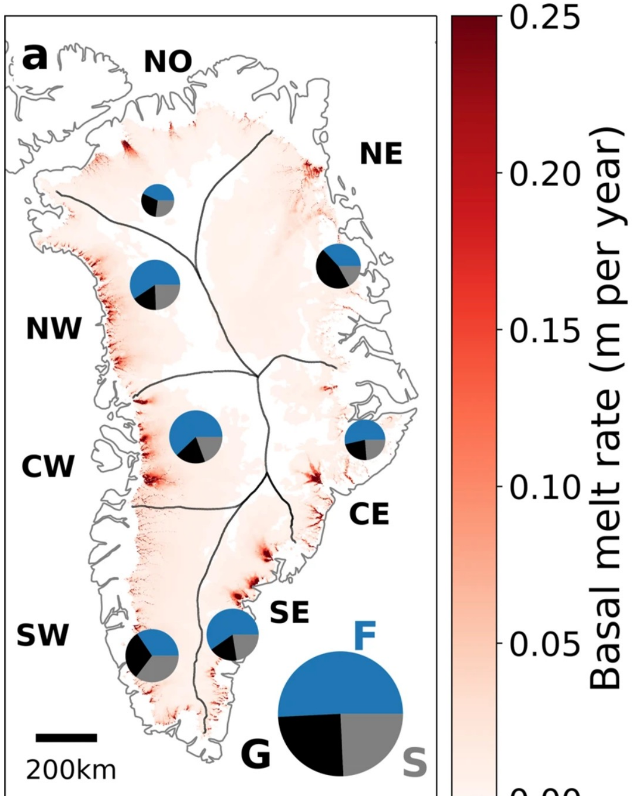

Karlsson et al. (2021)

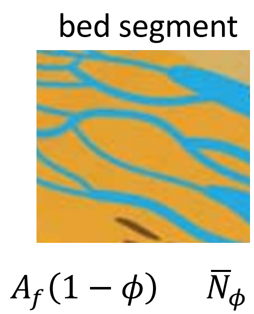

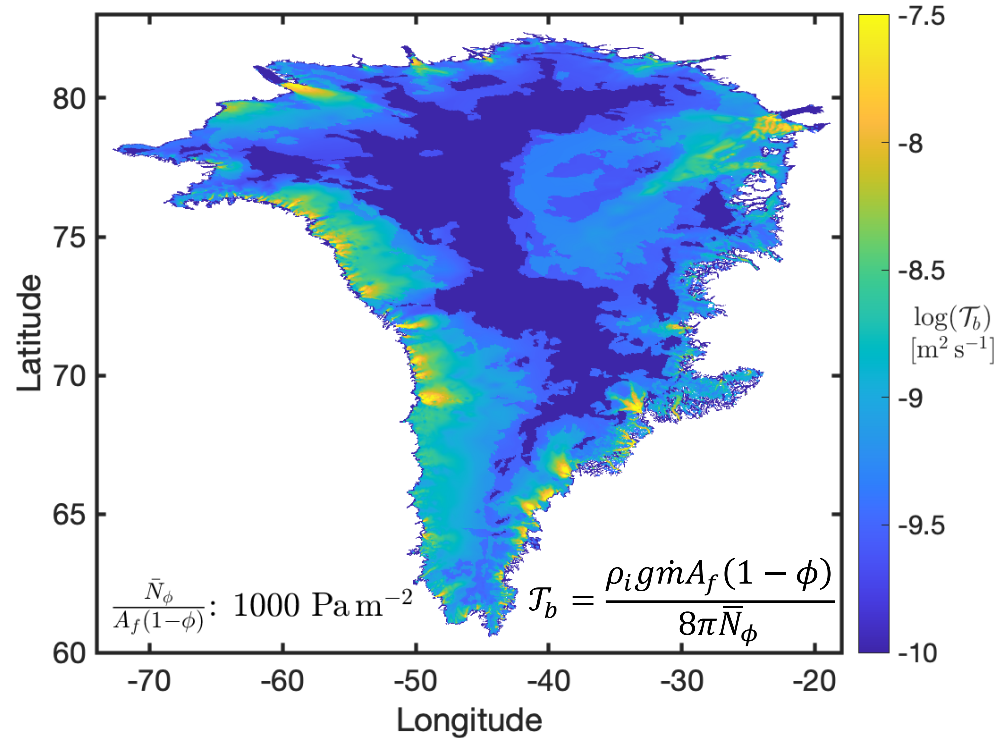

Maintaining $P_l = -\sigma_{\mathrm{nn}}$ while evacuating basal melt between conduits limits allowable transmissivity.

Transmissivity maxima for $P_l = -\sigma_{\mathrm{nn}}$ with idealized circular film elements of area A_f.

GEOLOGICAL SURVEY RESEARCH 1962

GROUND WATER

224. PERMEABILITY OF GLACIAL TILL

By STANLEY E. NORRIS, Columbus, Ohio

Work done in cooperation with the Division of Water of the Ohio Department of Natural Resources and with the Miami Conservancy District

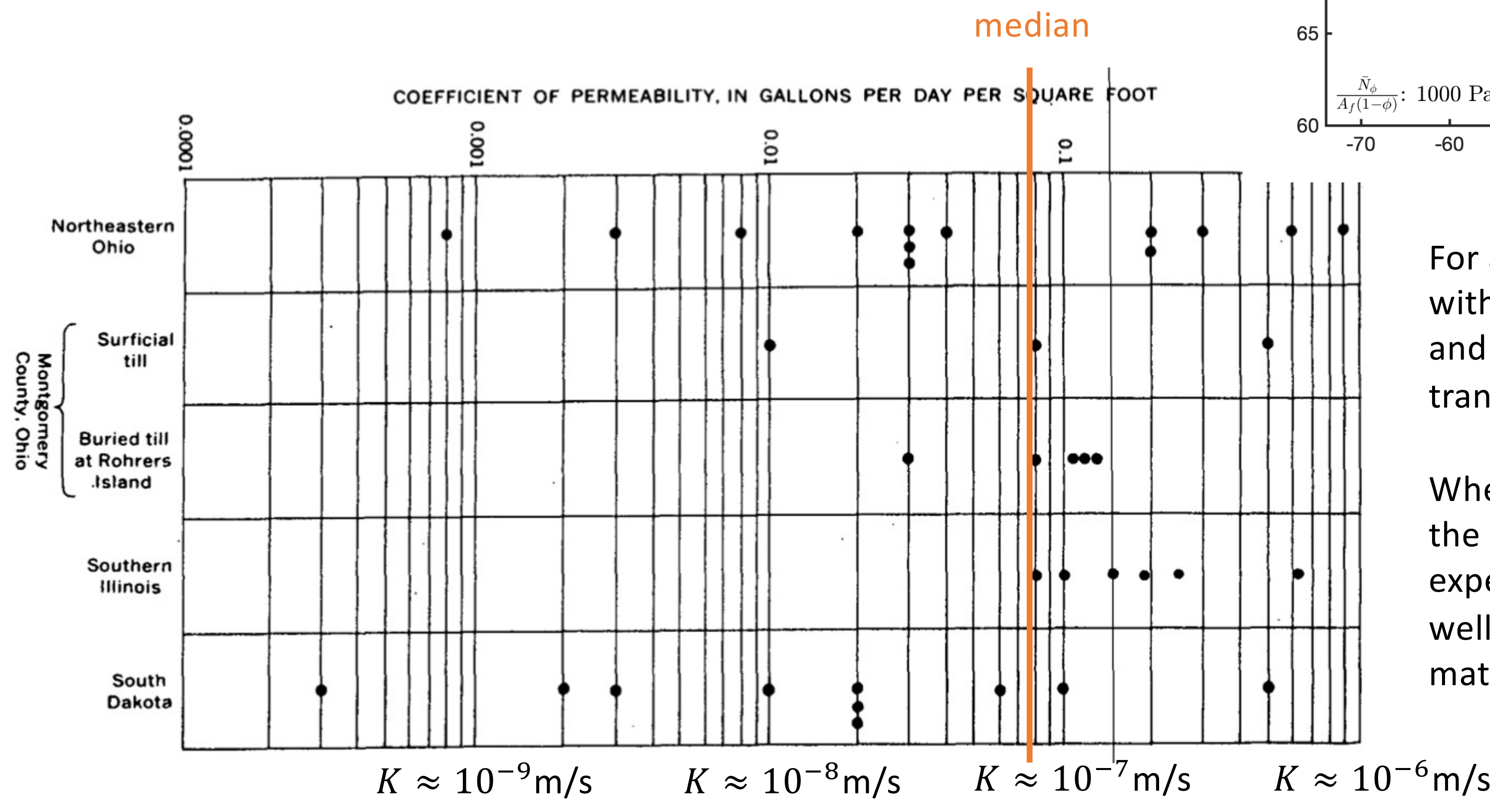

FIGURE 224.1.—Chart showing range of till permeability in Ohio, Illinois, and South Dakota.

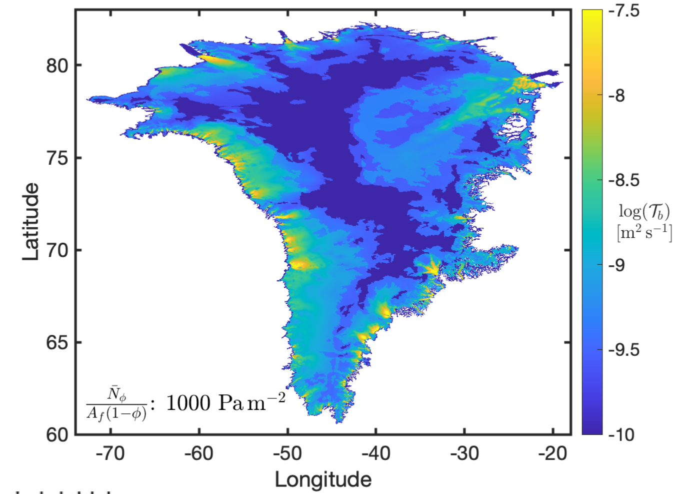

For a permeable medium with hydraulic conductivity K, and thickness h, the transmissivity is $\mathcal{T} = Kh$.

Where m-scale till layers line the basal interface, the bed is expected to be sufficiently well-drained that P_f cannot match ice normal stress.

Evidence for direct ice–bed coupling ($\sigma_{\text{eff}} > 0$) IV: mechanical

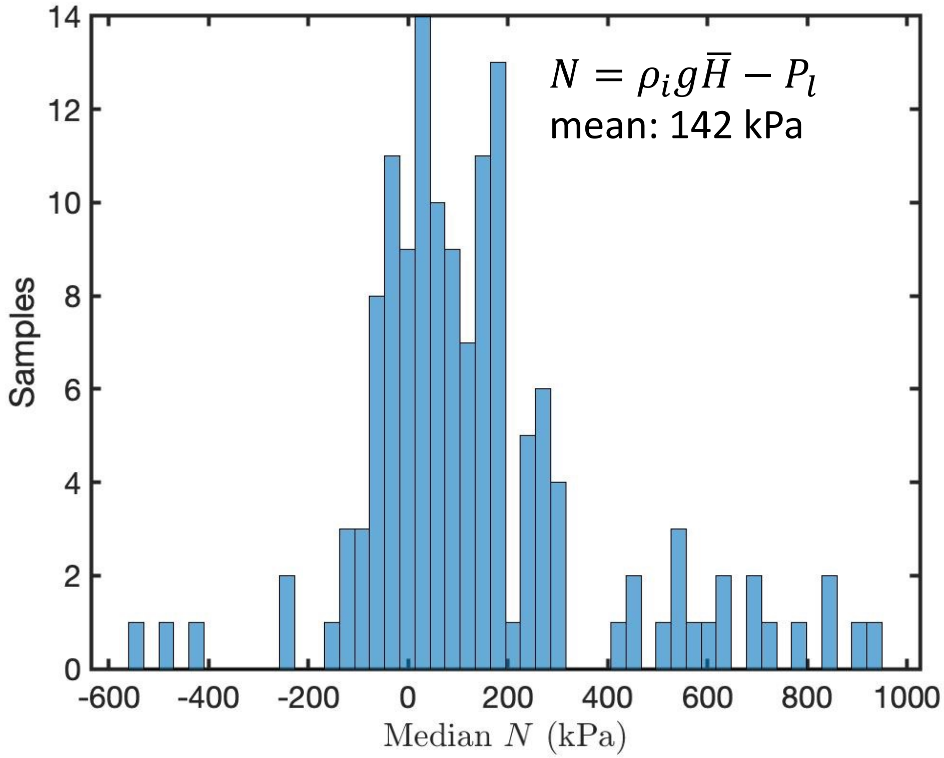

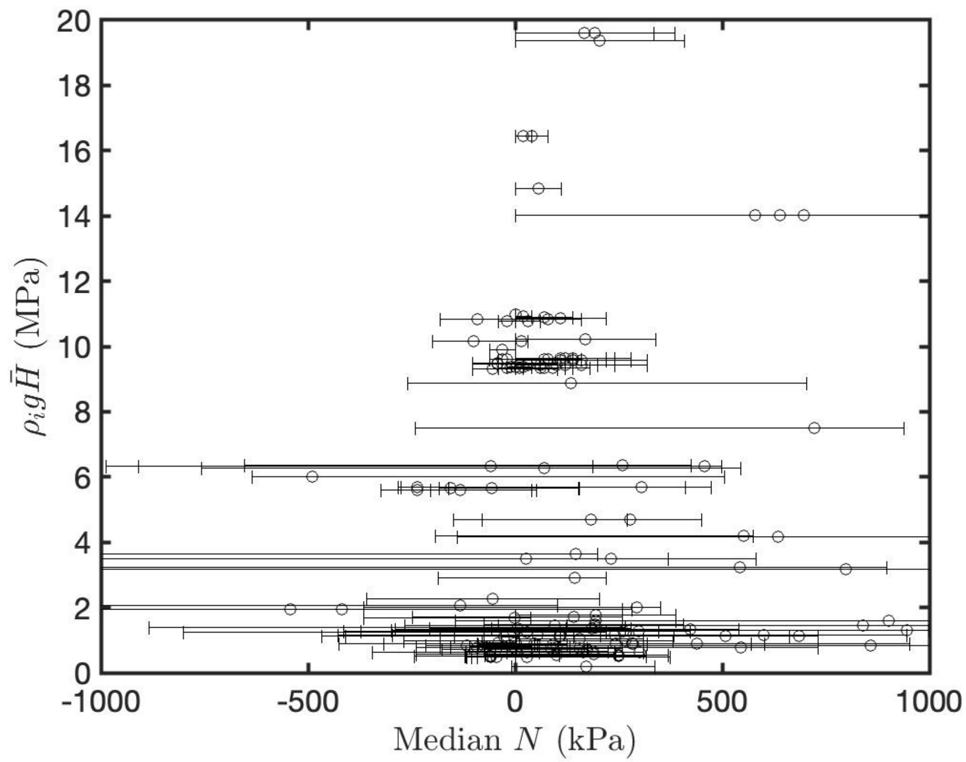

Closed: $\sigma_{\text{eff}} = 0$ requires $P_l = -\sigma_{\text{nn}}$; since $-\overline{\sigma \cdot \hat{\mathbf{n}}} = \rho_i g \overline{H} \hat{\mathbf{z}} - \tau \hat{\mathbf{x}}$, this would suggest $\overline{N} = \overline{\rho_i g \overline{H} - P_l} \approx \tau$.
Open: $\tau \approx f \sigma_{\text{eff}}$ for an effective friction coefficient $f \approx 0.5$ would suggest $\overline{N} \approx \tau / f$.

139 published borehole measurement time series appear inconsistent with $\overline{N} \approx \tau \approx 70$ kPa (t-score: 3.4, p≈0).
The average of compiled median $\overline{N}$ is 142 kPa, which is consistent with $\overline{N} \approx \tau / f \approx 140$ kPa (t-score: 0.1, p≈0.92).

Evidence for direct ice–bed coupling ($\sigma_{\text{eff}} > 0$) V: geological

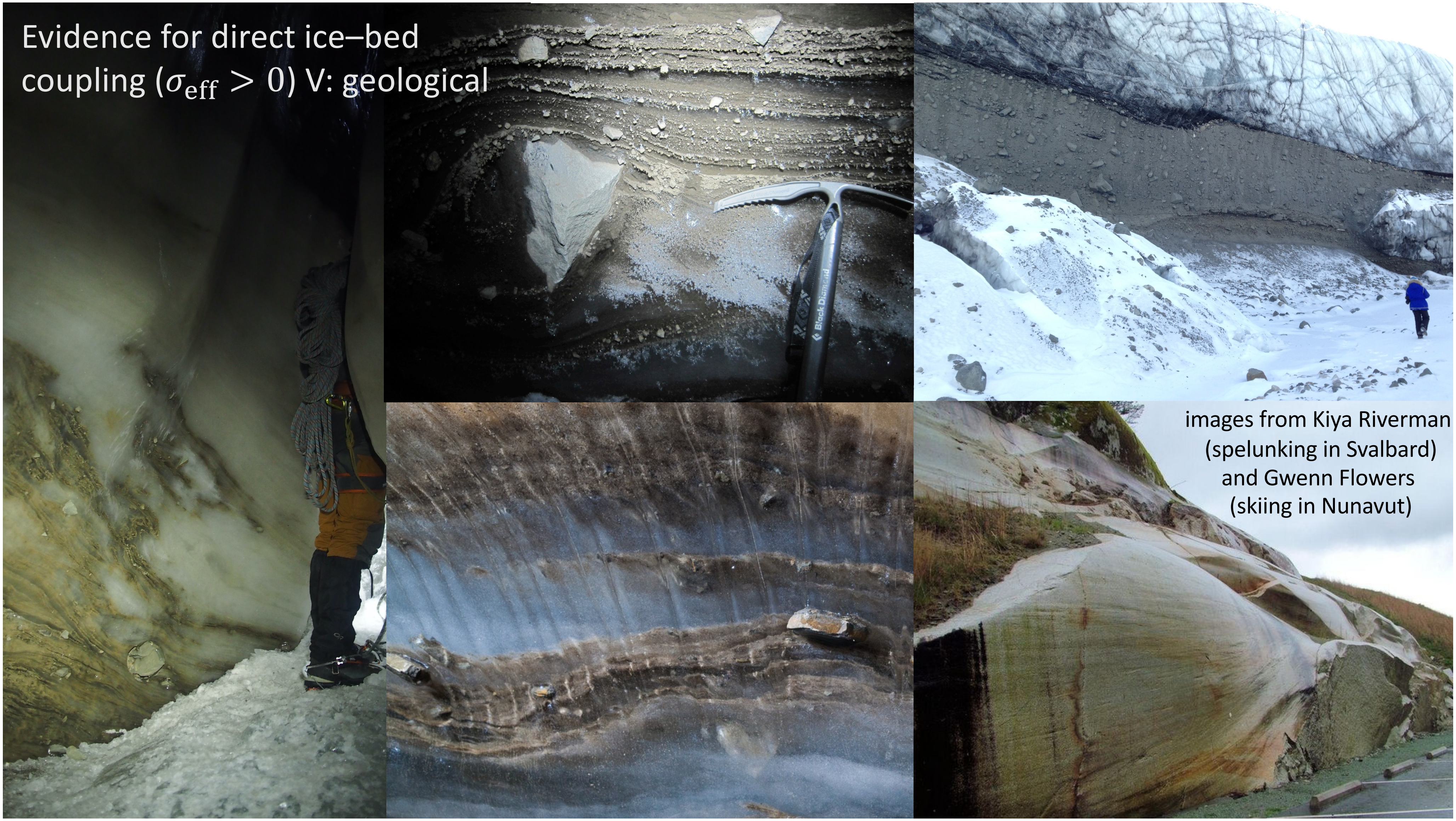

images from Kiya Riverman (spelunking in Svalbard) and Gwenn Flowers (skiing in Nunavut)

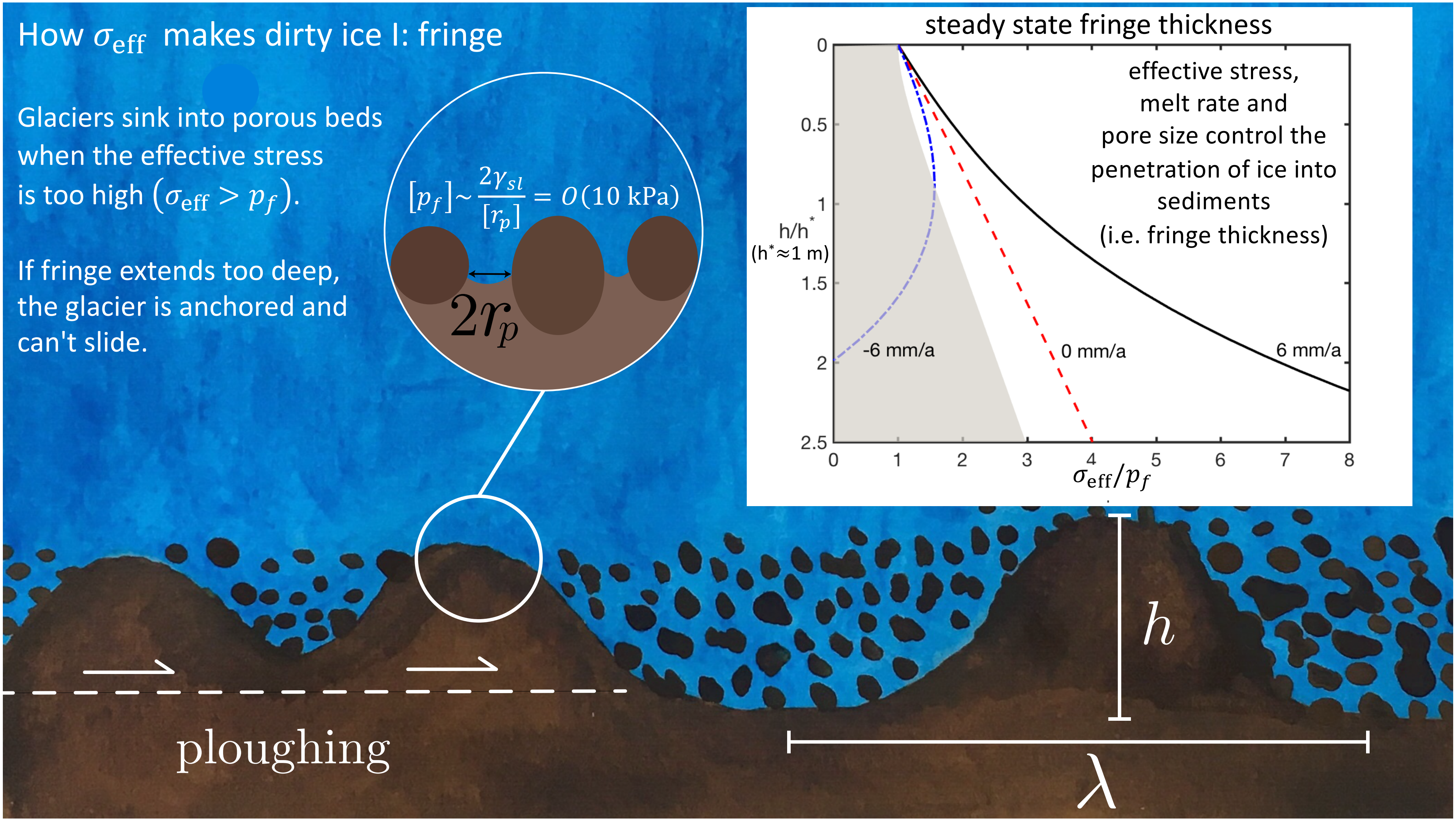

How σ_{eff} makes dirty ice I: fringe
Glaciers sink into porous beds when the effective stress is too high $(\sigma_{\text{eff}} > p_f)$.
If fringe extends too deep, the glacier is anchored and can't slide.
$[p_f] \sim \frac{2\gamma_{sl}}{[r_p]} = O(10 \text{ kPa})$
$2r_p$
steady state fringe thickness
effective stress, melt rate and pore size control the penetration of ice into sediments (i.e. fringe thickness)
h/h*
(h*≈1 m)
σ_{eff}/p_f
-6 mm/a
0 mm/a
6 mm/a
0
0.5
1
1.5
2
2.5
0
1
2
3
4
5
6
7
8
h
λ
ploughing

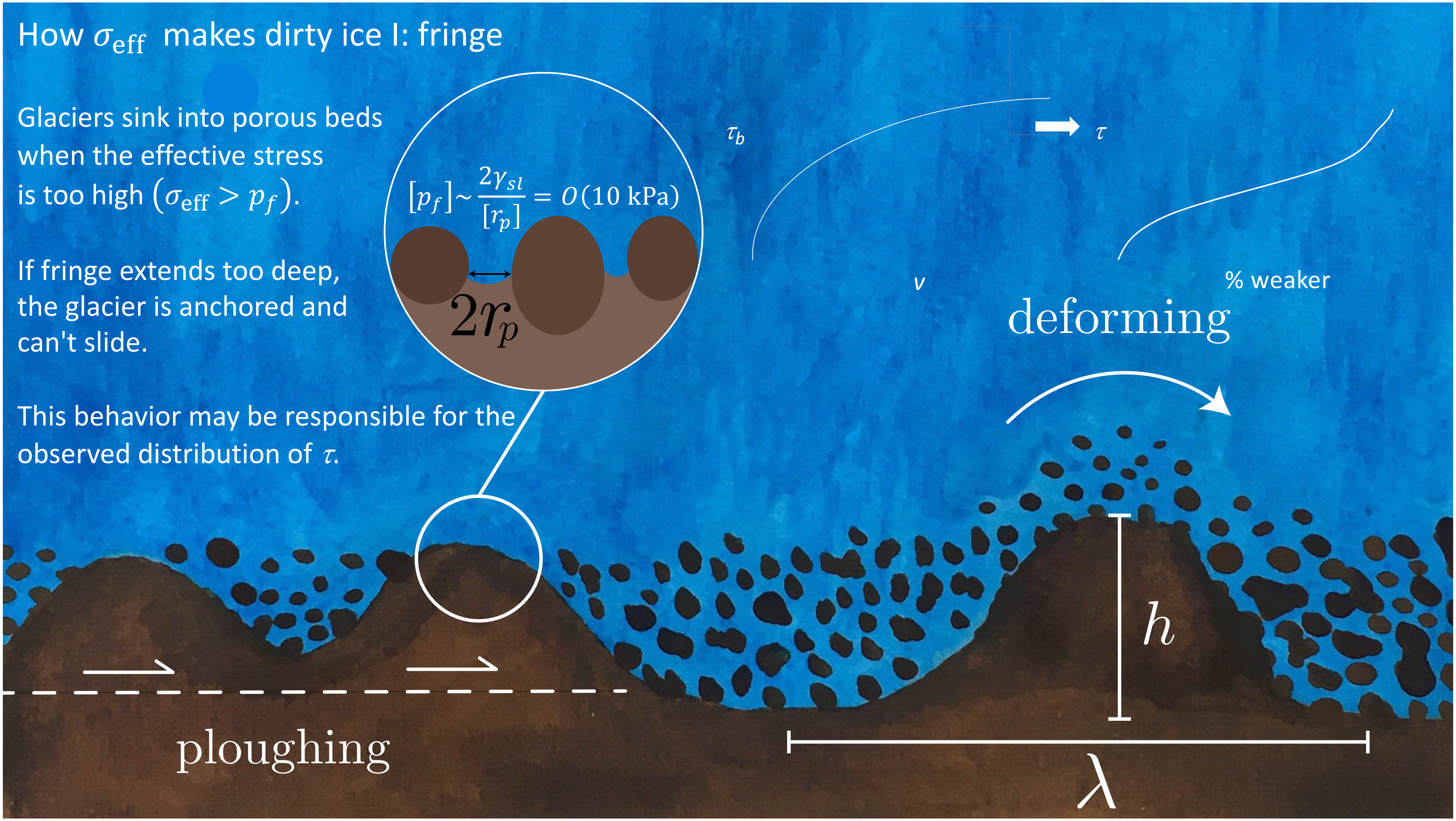
How σ_{eff} makes dirty ice I: fringe
Glaciers sink into porous beds when the effective stress is too high $(\sigma_{\mathrm{eff}} > p_f)$.
If fringe extends too deep, the glacier is anchored and can't slide.
This behavior may be responsible for the observed distribution of τ.
$[p_f] \sim \frac{2\gamma_{sl}}{[r_p]} = O(10\ \mathrm{kPa})$
$2r_p$
τ_b
τ
v
% weaker
deforming
ploughing
h
λ

How σ_{eff} makes dirty ice I: fringe

Dougal Hansen's experiments in Luke Zoet's lab in UW Madison.

Prediction: fringe growth when $\sigma_{eff} > P_f = 2\gamma_{il}/r_p$

Controlled P_{ice}–P_{water}=N(=σ_{eff}), bed materials, v_{ice} or τ.

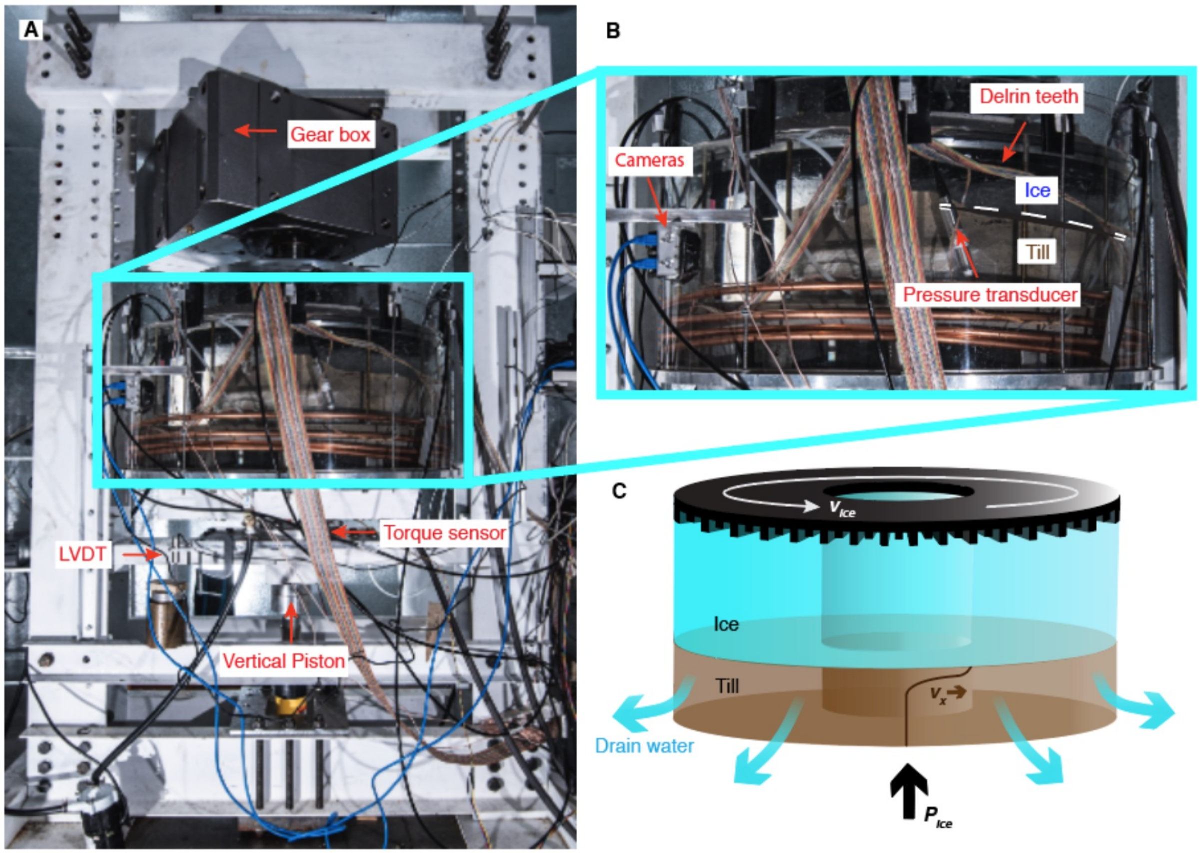

How σ_{eff} makes dirty ice I: fringe

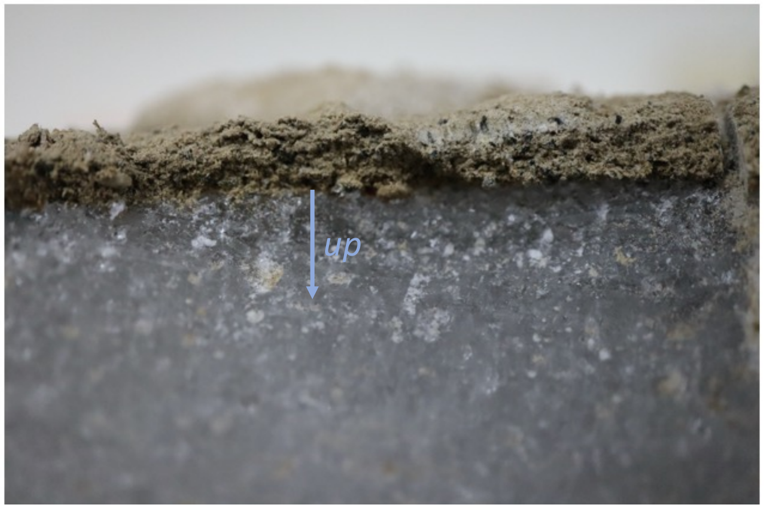

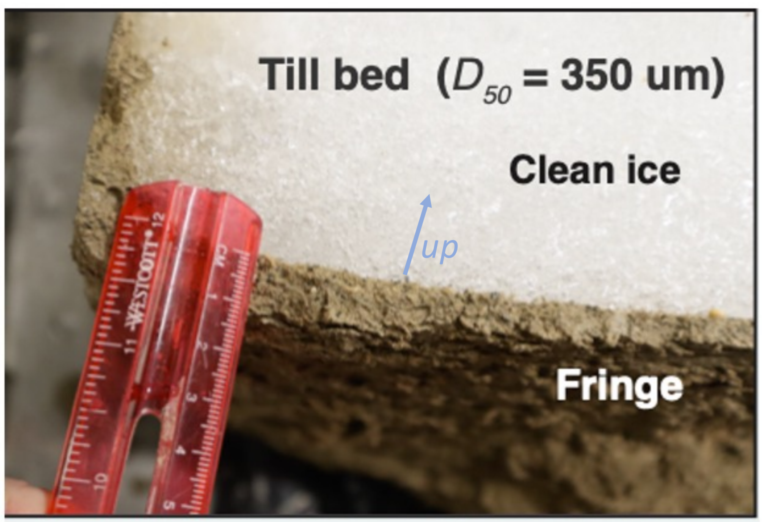

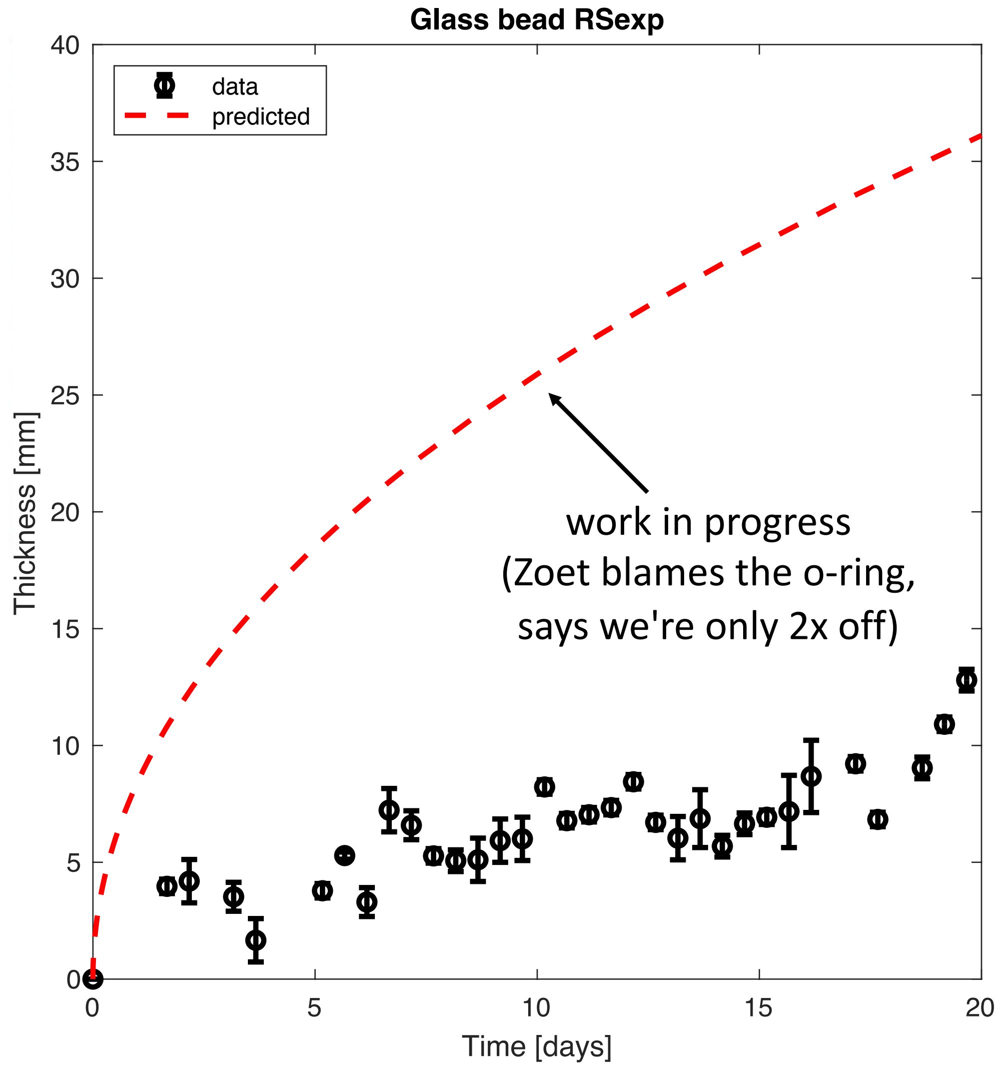

How σ_{eff} makes dirty ice II: veins

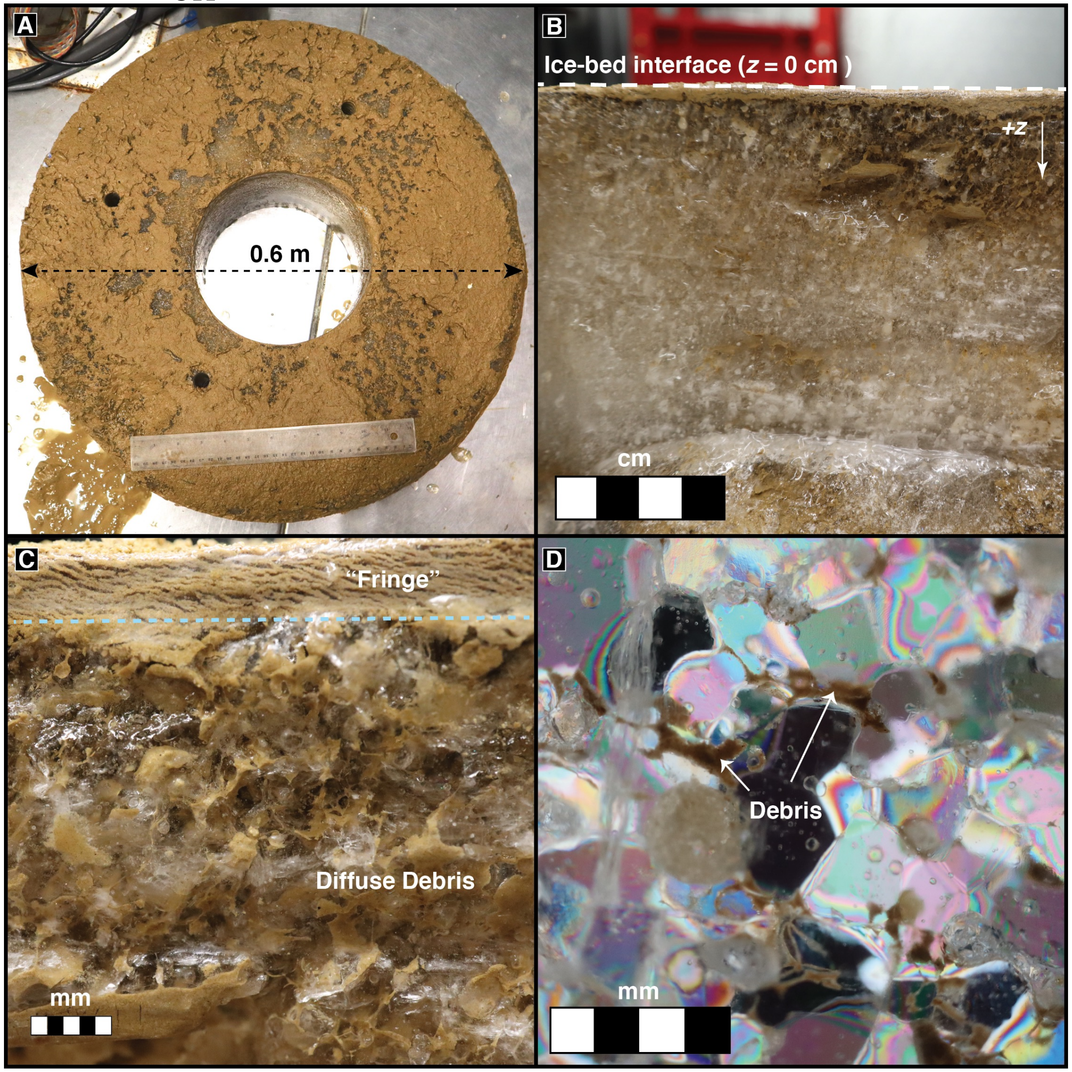

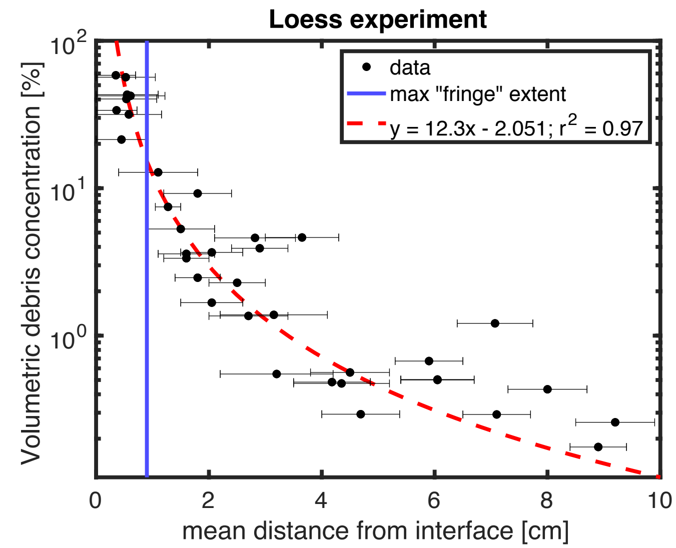

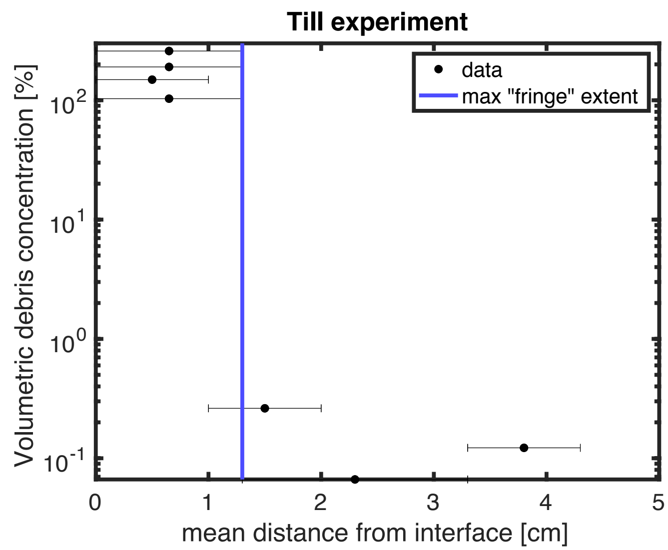

How σ_{eff} makes dirty ice II: veins

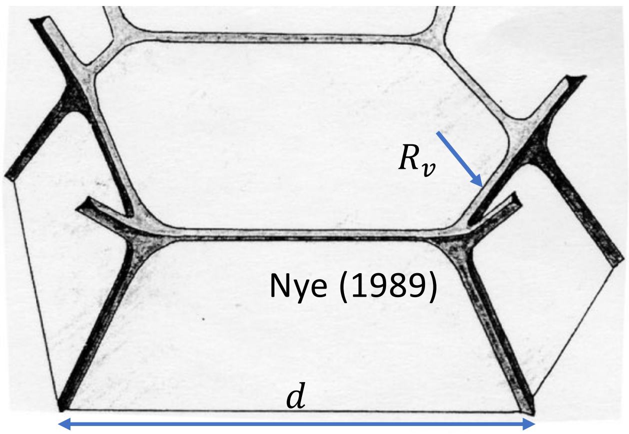

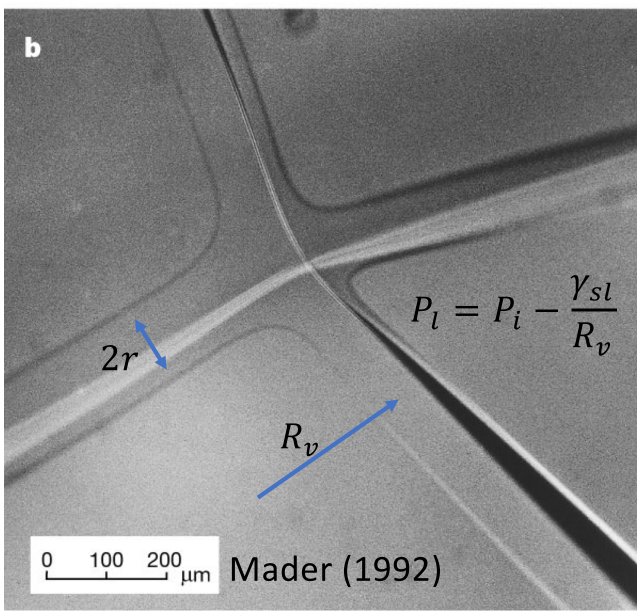

solute

Phase behavior: $T \approx T_m \left[1 - \frac{\gamma_{sl}}{\rho_s L R_v} - \frac{P_l - P_m}{\rho_s \rho_l L}(\rho_l - \rho_s)\right] - \Gamma c$

Liquid content (or R_v) is a function of T, c, (and elevation):

$$\tilde{\phi} \approx \left(\frac{1-\mathrm{C}}{1-\tilde{T}-\mathrm{C}\tilde{c}+\tilde{z}-\mathrm{C}\tilde{z}}\right)^2$$

Liquid flows towards colder, fresher ice (and lower non-hydrostatic P_i).

$$\frac{\tilde{q}}{\tilde{\phi}} = -\beta\tilde{\phi}\left(\frac{\partial \tilde{T}}{\partial \tilde{z}} + \mathrm{C}\frac{\partial \tilde{c}}{\partial \tilde{z}}\right).$$

Flow can mobilize small particles and drag them along veins.

Gradients in T, and c evolve and are coupled through dependence on ϕ.

$$\frac{\partial \tilde{T}}{\partial \tilde{t}} = \frac{\partial^2 \tilde{T}}{\partial \tilde{z}^2} - \mathrm{S}\phi_0 \frac{\partial \tilde{\phi}}{\partial \tilde{t}}$$

$$\frac{\partial \tilde{c}}{\partial \tilde{t}} = \frac{1}{L_e \tilde{\phi}} \frac{\partial}{\partial \tilde{z}}\left(\tilde{\phi}\frac{\partial \tilde{c}}{\partial \tilde{z}}\right) - \frac{\tilde{c}}{\tilde{\phi}}\frac{\partial \tilde{\phi}}{\partial \tilde{t}} - \frac{\tilde{q}}{\tilde{\phi}}\frac{\partial \tilde{c}}{\partial \tilde{z}}$$

How σ_{eff} makes dirty ice II: veins

Step change in basal temperature (e.g. as σ_{eff} changes abruptly) causes imbalance in liquid potential.

Liquid flows from warm, salty to cold, fresh.

Viable for diffuse debris entrainment in the bottom few meters.

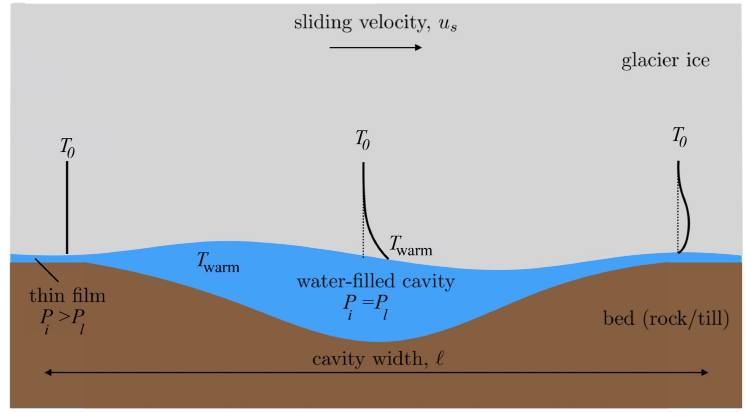

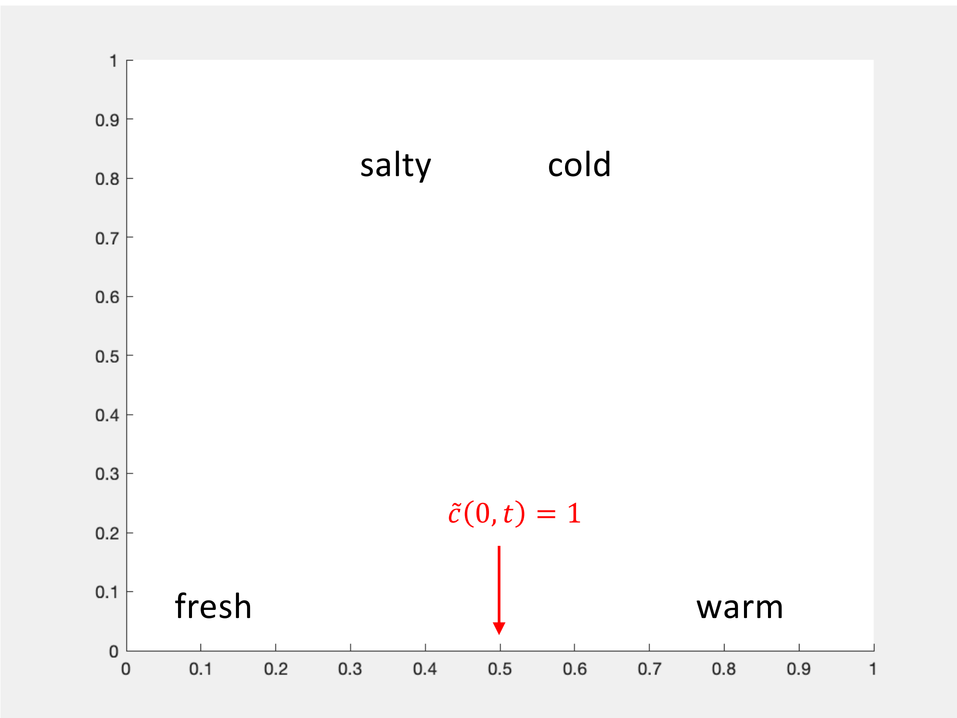

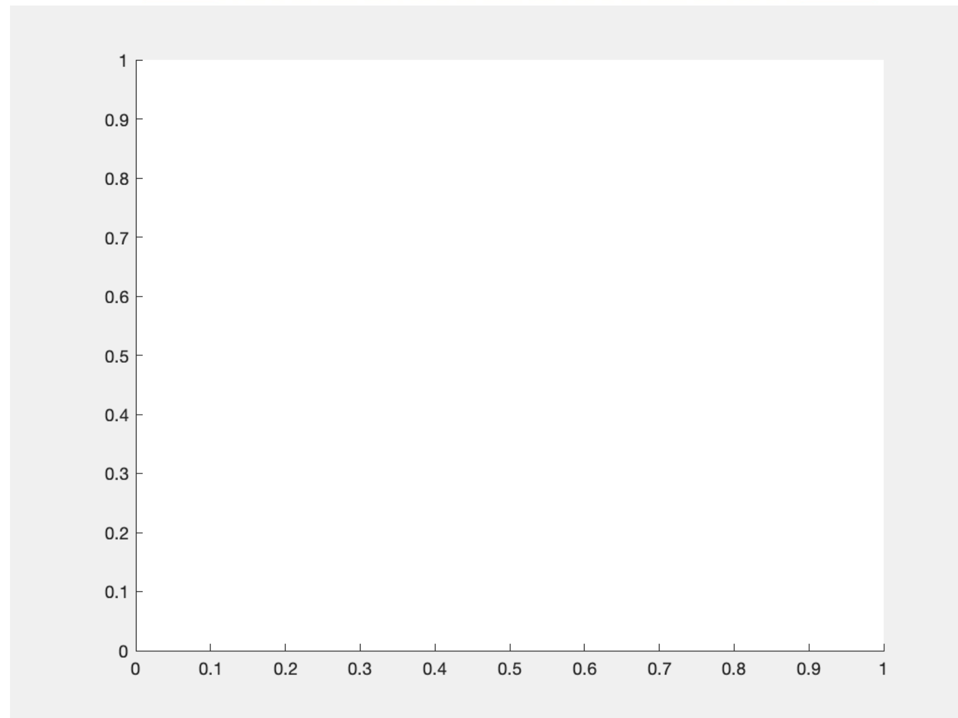

How σ_{eff} makes dirty ice II: veins

Experiment begins with thermal transient needed to freeze-in delrin teeth.

Relaxation produces upwards flow followed by slower downwards transport.

Experiments: ~~till~~, loess↑, glass beads↑↓

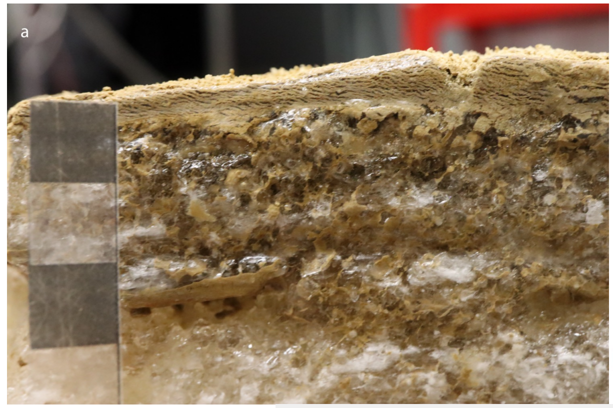

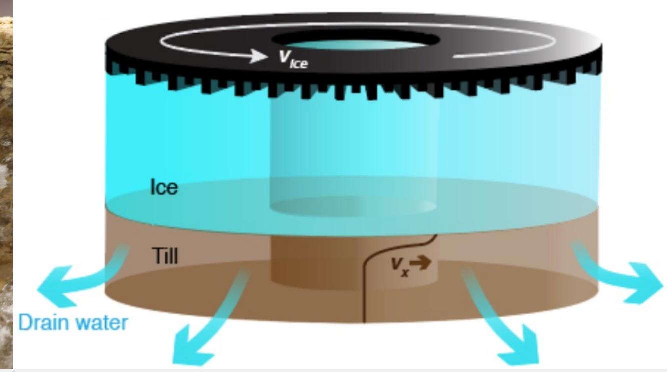

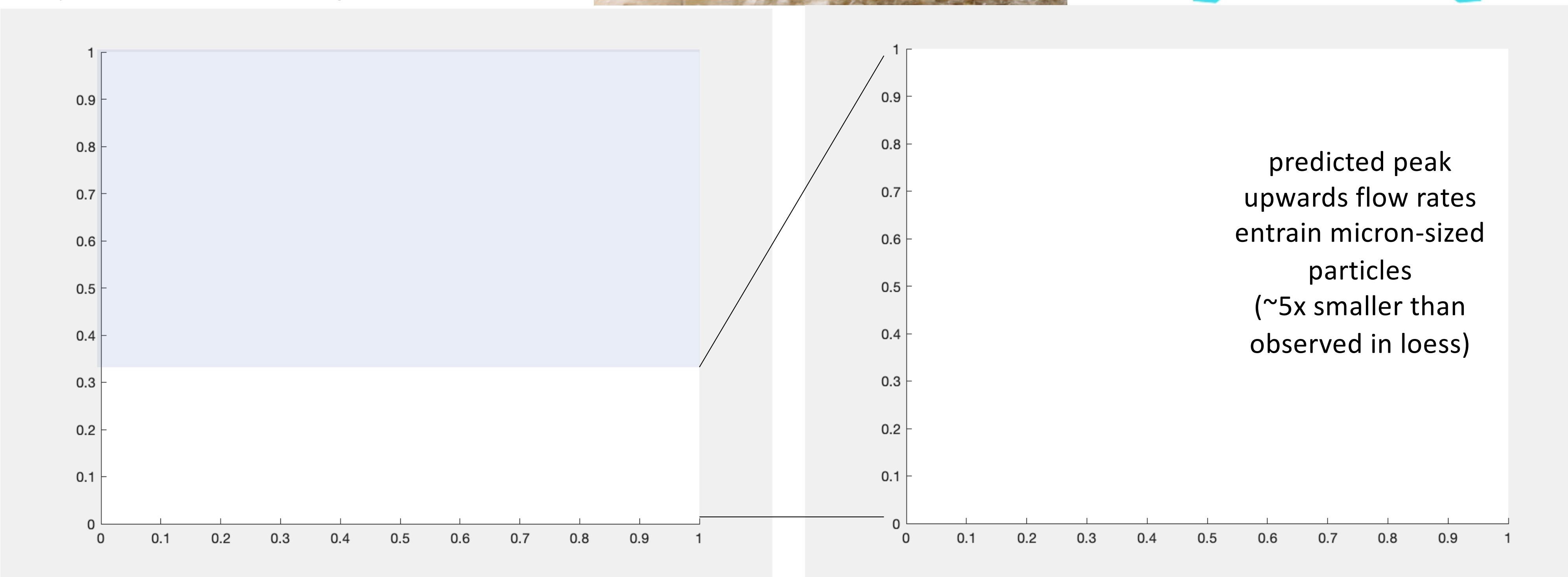

How σ_{eff} makes dirty ice III: unloading

Russell glacier, Greenland
Knight (1995)

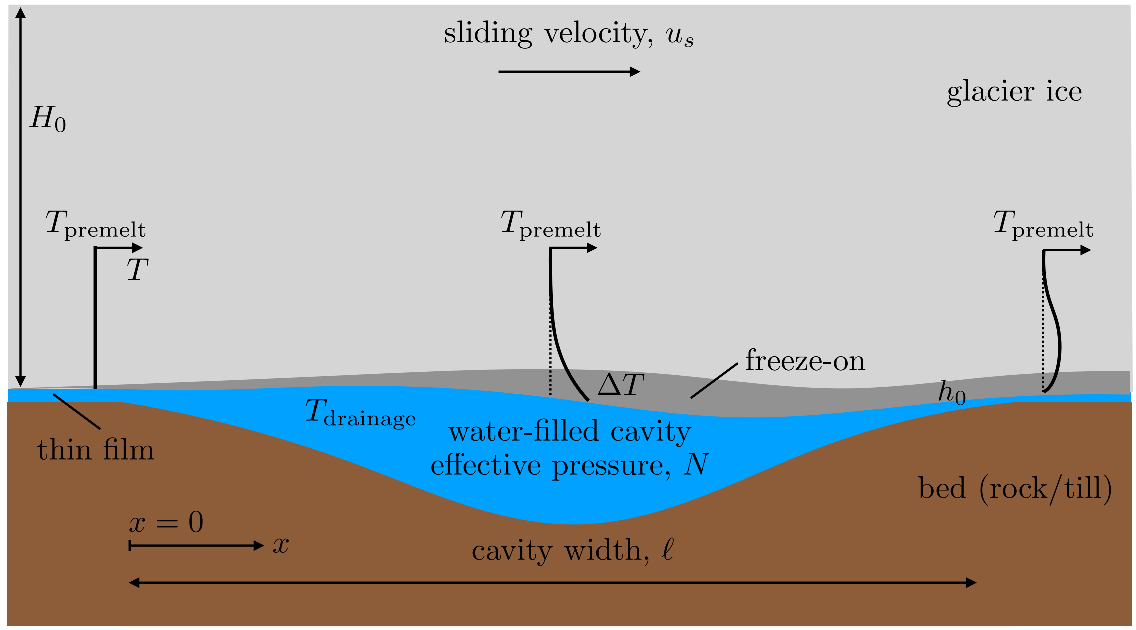

- ice slides over cavity and warms from $T_{\text{premelt}} \rightarrow T_{\text{drainage}}$ as $\sigma_{\text{eff}} \rightarrow 0$
- conductive heat transport drives freeze-on, reaching thickness h_0
- dissipation breaks symmetry, slower melting on reloading

  → net freeze on as long as cavities <50% of bed

How σ_{eff} makes dirty ice III: unloading

For a **single cavity**, freeze-on is

$$h_0 = \frac{2}{\sqrt{\pi}} \frac{C_p \Delta T}{\mathcal{L}} \sqrt{\frac{\kappa \ell}{u_s}}$$

and, combined with a simple cavity model, gives h_0 between 0.1 and 10 mm.

Extended to **cavity sequences** of dimension ℓ and spacing $\frac{\phi}{\ell}$, this predicts

$$h_{\min} \approx \frac{h_0 \sqrt{\phi}}{2} \sum_{j=1}^{J} \frac{1}{\sqrt{j}}$$

or

$$h_{\min} \approx \left(0.4\ \mathrm{m}^{\frac{1}{2}} \mathrm{Pa}^{\frac{1}{2}}\right) \phi_{\text{ref}} \sqrt{\frac{x}{\sigma_{\text{eff}}}}\,.$$

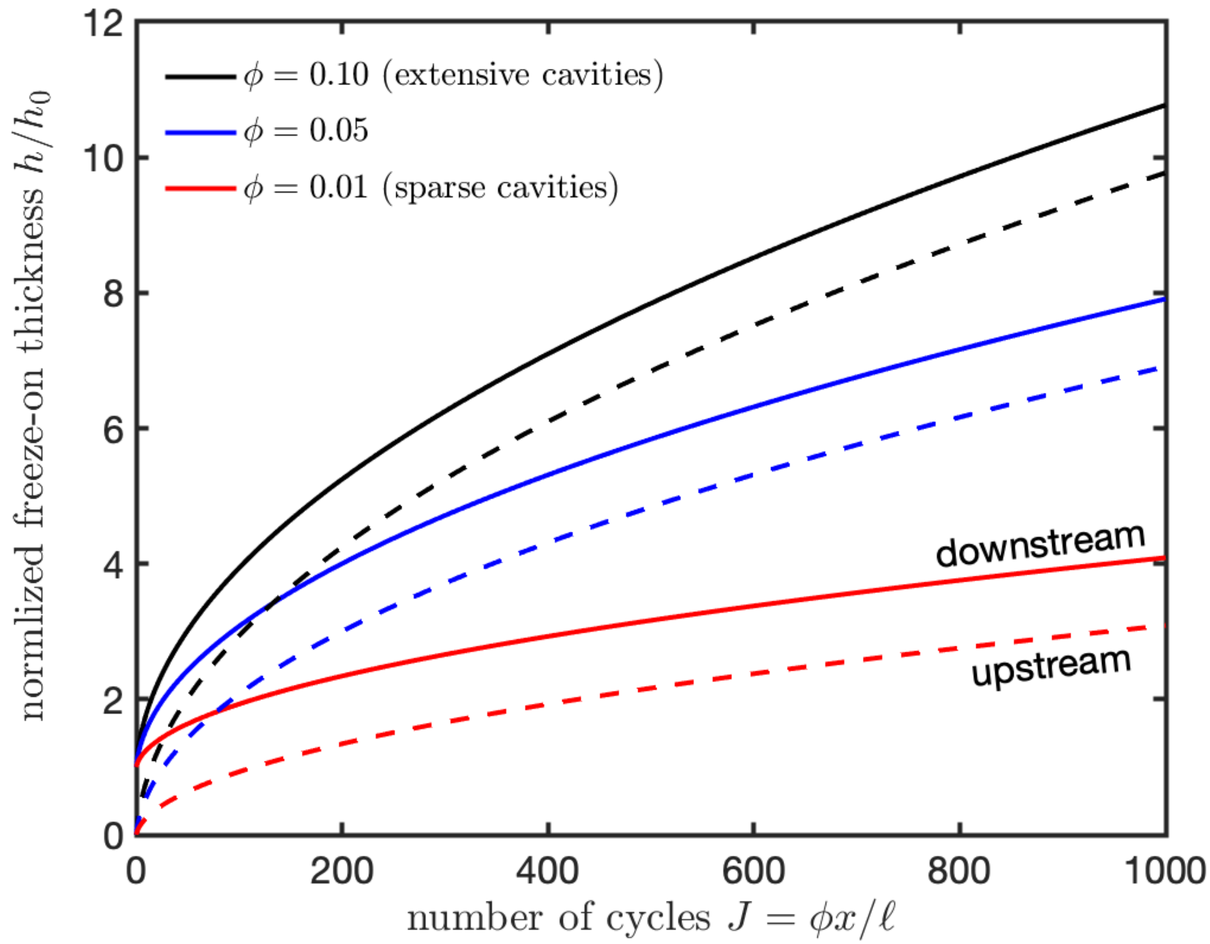

(e.g. $h_{\min}$= 0.1 m after sliding 100 km with σ_{eff}= 10 kPa and ϕ_{ref}= 8 %)

How σ_{eff} makes dirty ice III: unloading

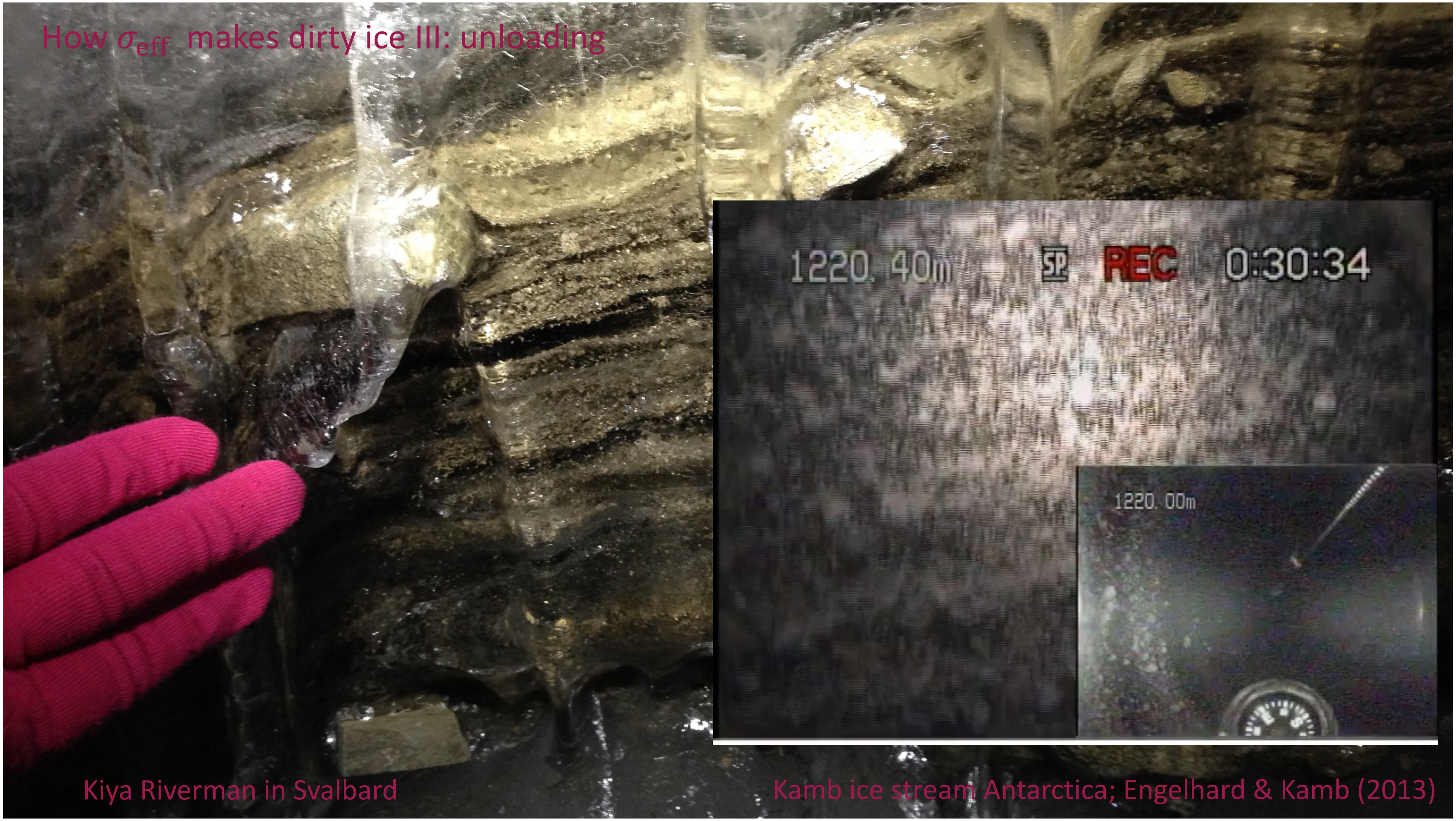

Kiya Riverman in Svalbard

Kamb ice stream Antarctica; Engelhard & Kamb (2013)

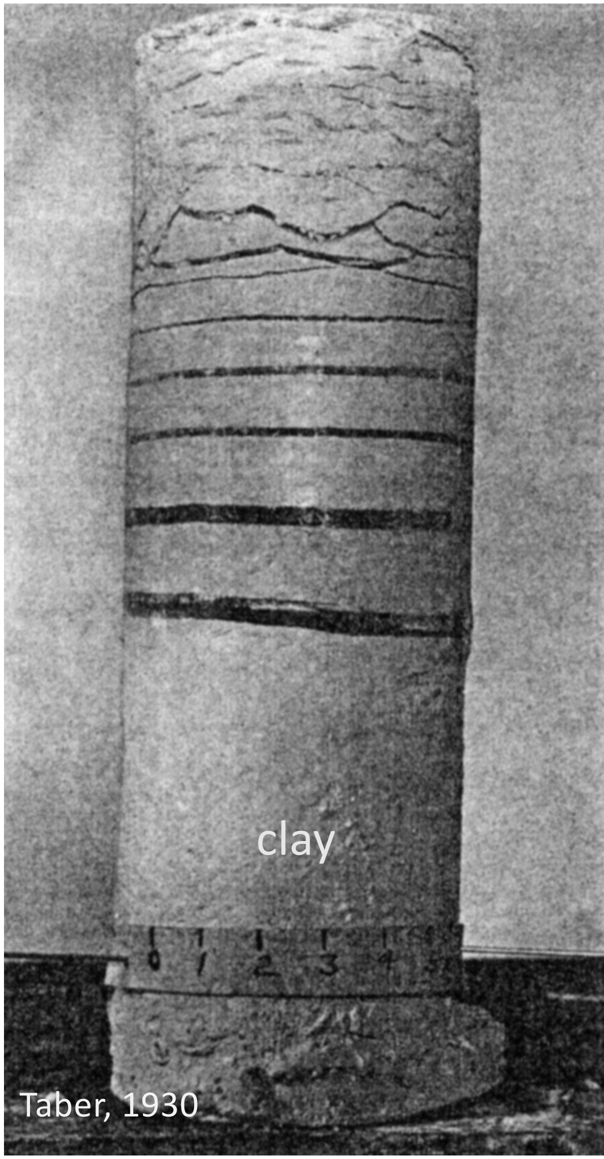
clay
Taber, 1930


Ystenes photo, near Trondheim


Meyer photo, subglacial tunnel


B
chalk
Matsuoko and Murton, 2008


Page photo, near Whistler

Sources (ordered by slide number of first appearance)

2 Taber, S. (1930). The mechanics of frost heaving. *The Journal of Geology*, *38*(4), 303-317.
Matsuoka, N., & Murton, J. (2008). Frost weathering: recent advances and future directions. *Permafrost and Periglacial Processes*, *19*(2), 195-210.
5 Rempel, A. W. (2007). Formation of ice lenses and frost heave. *Journal of Geophysical Research: Earth Surface*, *112*(F2).
6 Meyer, C. R., Schoof, C., & Rempel, A. W. (2023). A thermomechanical model for frost heave and subglacial frozen fringe. *J. Fluid Mech.* in press.
9 Kim, Y., Kimball, J.S., Glassy, J., and Du, J. (2017) An extended global earth system data record on daily landscape freeze–thaw status determined from satellite passive microwave remote sensing. Earth System Science Data 9 (1): 133–147.
10 Church, J. A., & White, N. J. (2011). Sea-level rise from the late 19th to the early 21st century. *Surveys in geophysics*, *32*, 585-602.
13 Sun, S., Pattyn, F., Simon, E. G., Albrecht, T., Cornford, S., Calov, R., ... & Zhang, T. (2020). Antarctic ice sheet response to sudden and sustained ice-shelf collapse (ABUMIP). *Journal of Glaciology*, *66*(260), 891-904.
14 Morlighem, M., Seroussi, H., Larour, E., & Rignot, E. (2013). Inversion of basal friction in Antarctica using exact and incomplete adjoints of a higher-order model. *Journal of Geophysical Research: Earth Surface*, *118*(3), 1746-1753.
15 Hoffman, M. J., Perego, M., Price, S. F., Lipscomb, W. H., Zhang, T., Jacobsen, D., ... & Bertagna, L. (2018). MPAS-Albany Land Ice (MALI): a variable-resolution ice sheet model for Earth system modeling using Voronoi grids, Geosci. Model Dev., 11, 3747–3780.
Hunter, P., Meyer, C., Minchew, B., Haseloff, M., & Rempel, A. (2021). Thermal controls on ice stream shear margins. *Journal of Glaciology*, *67*(263), 435-449.
16 Mouginot, J., Rignot, E., Scheuchl, B., & Millan, R. (2017). Comprehensive annual ice sheet velocity mapping using Landsat-8, Sentinel-1, and RADARSAT-2 data. *Remote Sensing*, *9*(4), 364.
Fretwell, P., Pritchard, H. D., Vaughan, D. G., Bamber, J. L., Barrand, N. E., Bell, R., ... & Zirizzotti, A. (2013). Bedmap2: improved ice bed, surface and thickness datasets for Antarctica. *The cryosphere*, *7*(1), 375-393.
Meyer, C. R., Downey, A. S., & Rempel, A. W. (2018). Freeze-on limits bed strength beneath sliding glaciers. *Nature communications*, *9*(1), 3242.
18 Zoet, L. K., & Iverson, N. R. (2015). Experimental determination of a double-valued drag relationship for glacier sliding. *Journal of Glaciology*, *61*(225), 1-7.
Zoet, L. K., & Iverson, N. R. (2020). A slip law for glaciers on deformable beds. *Science*, *368*(6486), 76-78.
Minchew, B., & Joughin, I. (2020). Toward a universal glacier slip law. *Science*, *368*(6486), 29-30.
19 Schoof, C. (2010). Ice-sheet acceleration driven by melt supply variability. *Nature*, *468*(7325), 803-806.
Ashmore, D. W., & Bingham, R. G. (2014). Antarctic subglacial hydrology: current knowledge and future challenges. *Antarctic Science*, *26*(6), 758-773.
10 Style, R. W., Gerber, D., Rempel, A. W., & Dufresne, E. R. (2023). The generalized Clapeyron equation and its application to confined ice growth. *Journal of Glaciology*, in press.
21 Rempel, A. W., & Meyer, C. R. (2019). Premelting increases the rate of regelation by an order of magnitude. *Journal of Glaciology*, *65*(251), 518-521.
22 Helanow, C., Iverson, N. R., Woodard, J. B., & Zoet, L. K. (2021). A slip law for hard-bedded glaciers derived from observed bed topography. *Science Advances*, *7*(20), eabe7798.
23 Gajek, W., Gräff, D., Hellmann, S., Rempel, A. W., & Walter, F. (2021). Diurnal expansion and contraction of englacial fracture networks revealed by seismic shear wave splitting. *Communications Earth & Environment*, *2*(1), 209.
24 McDowell, I. E., Humphrey, N. F., Harper, J. T., & Meierbachtol, T. W. (2021). The cooling signature of basal crevasses in a hard-bedded region of the Greenland Ice Sheet. *The Cryosphere*, *15*(2), 897-907.
26 Karlsson, N. B., Solgaard, A. M., Mankoff, K. D., Gillet-Chaulet, F., MacGregor, J. A., Box, J. E., ... & Fausto, R. S. (2021). A first constraint on basal melt-water production of the Greenland ice sheet. *Nature Communications*, *12*(1), 3461.
27 Meyer, C., Rempel, A. W., Hansen, D., Stubblefield, A. G., & Zoet, L. (2022, December). Cataloging Effective Pressure and Frozen Fringe Under Glaciers. In *AGU Fall Meeting Abstracts* (Vol. 2022, pp. C22D-0790).
34 Nye, J. F. (1989). The geometry of water veins and nodes in polycrystalline ice. *Journal of Glaciology*, *35*(119), 17-22.
Mader, H. M. (1992). Observations of the water-vein system in polycrystalline ice. *Journal of Glaciology*, *38*(130), 333-347.
37 Knight, P. G. (1997). The basal ice layer of glaciers and ice sheets. *Quaternary Science Reviews*, *16*(9), 975-993.
Rempel, A. W., Meyer, C. R., & Riverman, K. L. (2022). Melting temperature changes during slip across subglacial cavities drive basal mass exchange. *J. Glaciology*, *68*(267), 197-203.
39 Engelhardt, H., & Kamb, B. (2013). Kamb Ice Stream flow history and surge potential. Annals of Glaciology, 54(63), 287-298.